(2)

REPORT DOCUMENTATION PAGE

Form Approved OMB No. 0704-0188

AD-A221 107

1a. REPORT SECURITY CLASSIFICATION: Unclassified	1b. RESTRICTIVE MARKINGS
	3. DISTRIBUTION/AVAILABILITY OF REPORT: Approved for public release, distribution unlimited
4. PERFORMING ORGANIZATION REPORT NUMBER(S): HTC-9001	5. MONITORING ORGANIZATION REPORT NUMBER(S): AFOSR-TR- 90-0386
6a. NAME OF PERFORMING ORGANIZATION: High Technology Corporation; 6b. OFFICE SYMBOL (If applicable):	7a. NAME OF MONITORING ORGANIZATION: AFOSR
6c. ADDRESS (City, State, and ZIP Code): 28 Research Drive, Hampton, VA 23666	7b. ADDRESS (City, State, and ZIP Code): Building 410, Bolling AFB, DC 20332-6448
8a. NAME OF FUNDING/SPONSORING ORGANIZATION: AFOSR; 8b. OFFICE SYMBOL (If applicable): NA	9 PROCUREMENT INSTRUMENT IDENTIFICATION NUMBER: F49620-89-C-0093
8c. ADDRESS (City, State, and ZIP Code): Building 410, Bolling AFB, DC 20332-6448	10. SOURCE OF FUNDING NUMBERS: PROGRAM ELEMENT NO. 61102F; PROJECT NO. 2307; TASK NO A2; WORK UNIT ACCESSION NO

11. TITLE (Include Security Classification)
Nonlinear Development of Gortler and Crossflow Vortices and Gortler/Tollmien-Schlichting Wave Interaction

12. PERSONAL AUTHOR(S)
M. R. Malik and A. A. Godil

13a. TYPE OF REPORT	13b TIME COVERED	14. DATE OF REPORT (Year, Month, Day)	15. PAGE COUNT
Final Report	FROM 7-1-89 TO 12-31-89	90-02-26	68

16. SUPPLEMENTARY NOTATION

17. COSATI CODES			18. SUBJECT TERMS (Continue on reverse if necessary and identify by block number)
FIELD	GROUP	SUB-GROUP	Stability, Transition, Gortler, Crossflow, Tollmien-Schlichting, Wave-Interaction

19. ABSTRACT (Continue on reverse if necessary and identify by block number)

The problem of nonlinear development of Görtler vortices on a curved wall is studied within the framework of incompressible Navier-Stokes equations which are solved by a Fourier-Chebyshev spectral method. The results show that higher harmonics grow due to nonlinear effects; however, most of the energy remains in the fundamental mode. The computed flow field in the presence of a Görtler vortex is in qualitative agreement with the experimental data. The interaction of the Görtler vortex with a two-dimensional Tollmien-Schlichting wave is also studied and it is shown that the Tollmien-Schlichting wave grows faster than its linear theory growth rate when the amplitude of the Görtler vortex is sufficiently large. Due to nonlinear effects this interaction further leads to the development of oblique waves with spanwise wavelength

20. DISTRIBUTION/AVAILABILITY OF ABSTRACT	21. ABSTRACT SECURITY CLASSIFICATION
☐ UNCLASSIFIED/UNLIMITED ☒ SAME AS RPT. ☐ DTIC USERS	Unclassified
22a. NAME OF RESPONSIBLE INDIVIDUAL: DR James McMichael	22b. TELEPHONE (Include Area Code): (202) 767-4936 / 22c. OFFICE SYMBOL: AFOSR/NA

Block 19 - Continued

equal to the Görtler vortex wavelength. The numerical method is also applied to study the nonlinear development of a stationary crossflow vortex in a Falkner-Skan-Cooke boundary layer. The crossflow vortex develops in a manner similar to that found earlier for rotating disk flow. The fundamental and the higher harmonics all tend to saturate when the integration is carried to large amplitudes. The computed velocity distribution clearly shows the emergence of the superharmonic which, however, does not dominate the fundamental mode. The Falkner-Skan-Cooke flow, modulated by the presence of the crossflow vortex, is found to be subject to a new secondary instability with large growth rates.

Nonlinear Development of Görtler and Crossflow Vortices and Görtler/Tollmien-Schlichting Wave Interaction

ABSTRACT

The problem of nonlinear development of Görtler vortices on a curved wall is studied within the framework of incompressible Navier-Stokes equations which are solved by a Fourier-Chebyshev spectral method. The results show that higher harmonics grow due to nonlinear effects; however, most of the energy remains in the fundamental mode. The computed flow field in the presence of a Görtler vortex is in qualitative agreement with the experimental data. The interaction of the Görtler vortex with a two-dimensional Tollmien-Schlichting wave is also studied and it is shown that the Tollmien-Schlichting wave grows faster than its linear theory growth rate when the amplitude of the Görtler vortex is sufficiently large. Due to nonlinear effects this interaction further leads to the development of oblique waves with spanwise wavelength equal to the Görtler vortex wavelength. The numerical method is also applied to study the nonlinear development of a stationary crossflow vortex in a Falkner-Skan-Cooke boundary layer. The crossflow vortex develops in a manner similar to that found earlier for rotating disk flow. The fundamental and the higher harmonics all tend to saturate when the integration is carried to large amplitudes. The computed velocity distribution clearly shows the emergence of the superharmonic which, however, does not dominate the fundamental mode. The Falkner-Skan-Cooke flow, modulated by the presence of the crossflow vortex, is found to be subject to a new secondary instability with large growth rates.

1. INTRODUCTION

The subject of laminar/turbulent boundary layer transition is of fundamental and practical importance in fluid mechanics. Depending upon the flow conditions and body geometry, various instability mechanisms such as Tollmien-Schlichting (TS), Görtler and crossflow may be operative and could also interact if multiple instability modes are present. A number of studies have been carried out to understand the breakdown of TS waves to turbulence in a flat-plate boundary layer. Notable among these are the experiments of Klebanoff et al. [1], Kachanov et al. [2], Saric & Thomas [3], the theoretical studies of Craik [4] and Herbert [5], and numerical simulations of Wray & Hussaini [6], Orszag & Patera [7], Spalart & Yang [8], Laurien & Kleiser [9], Zang & Hussaini [10] and Fasel et al. [11]. Because of these and other related studies, at least the early stages of the breakdown process are now relatively well-understood.

The boundary layer that develops on a concavely curved surface is subject to Görtler instability which manifests itself in the form of steady streamwise counter-rotating vortices. Similarly, near the leading edge of a swept wing, crossflow instability sets in due to inflectional crossflow velocity profiles. This instability is known to result in corotating steady vortices known as crossflow vortices which are oriented at small angles with the inviscid streamlines. Sometimes, this instability may also result in unsteady crossflow vortices. Depending upon flow parameters, Görtler/TS and crossflow/TS modes may coexist and mutually interact. This problem has received very little attention, even though it is of direct application in the design of modern aircrafts.

Experimental work on Görtler vortices has been performed for example, by Bippes & Görtler [12], Winoto & Crane [13] and Swearingen &

Blackwelder [14]. The work of the latter authors was particularly carried out to understand the details of the growth and breakdown of Görtler vortices and eventual transition to turbulence. The results showed the development of low speed regions, between the counter-rotating vortices, which project outside the nominal Blasius boundary layer and create strong inflectional normal and spanwise velocity profiles. These profiles develop secondary instabilities resulting in unsteady oscillations prior to transition. Two types of secondary instability were identified. The first results in a horse-shoe vortex structure also found by Aihara & Koyama [15]. The second type of instability results in sinuous transverse oscillations which were earlier reported by Bippes [16]. Both modes were also observed in the experiment of Jeans & Johnston [17]

Crossflow instability in swept-wing flows was first discovered by Gray [18] and later the work of Owen & Randall [19] and Gregory et al. [20] made the phenomenon more clear and also provided a theoretical basis for appearance of this instability in general three-dimensional boundary layers. Experimental investigations into this instability in rotating disk flow were performed by Smith [21], Gregory et al. [20] and Wilkinson & Malik [22], among others. Due to three-dimensional basic flow, questions still remain about the nature of the instability even in the linear regime. Historically, it had been believed that this instability would only result in steady crossflow vortices. However, the work of Malik & Poll [23] pointed out that small unsteady disturbances may also play an important role in the transition process in these flows. Since then, a number of studies have been initiated to understand the nature of the swept-wing boundary layer instability at its linear and nonlinear stage. Notable among these are the experiments of Müller & Bippes [24] and Dagenhart et al. [25]. Both the

stationary and unsteady disturbances were observed in these experiments which concern low-speed flows. Earlier, Saric & Yeates [26] only found stationary crossflow vortices. However, they observed that at some distance downstream from the leading edge a superharmonic appears in the hot-wire signal. The amplitude of the superharmonic was found to be three times the amplitude of the fundamental. Reed [27] attempted to explain this phenomenon by using her wave-interaction theory. Numerical simulations of the early nonlinear stages of the crossflow vortex have been performed by Malik [28] and recently by Meyer & Kleiser [29].

The Görtler/TS interaction problem has been studied by Malik [30] using numerical methods, Hall & Smith [31] using asymptotic methods and Nayfeh & Al-Maaitah [32] using the method of multiple scales. Questions still remain that at what amplitudes such interactions take place. An understanding of these interactions will also shed some light on the crossflow/TS interaction problem. The practical interest in these interaction studies arises from their relevance in boundary layer transition prediction which is needed for the design of modern aircrafts. The state of the art technique used for transition prediction is based upon linear theory in the form of the e^N method. If wave-interactions of the type discussed above were to take place, they will render the prediction of the e^N method useless and will have disastrous consequences for the design of laminar flow control wings. It is, therefore, important to understand the nature of these wave interactions and determine the parameter space within which they might take place.

In the present report, we use a Fourier/Chebyshev spectral method to investigate the nonlinear development of a Görtler vortex. The computed flow field is compared with the experiments of Swearingen & Blackwelder

[14]. The numerical method is then used to study the interaction of a small amplitude TS wave with a finite-amplitude Görtler vortex. Finally, nonlinear development of a steady crossflow vortex is considered and the emergence of a secondary instability is discussed.

2. GOVERNING EQUATIONS AND NUMERICAL APPROACH

We consider the problem of laminar/turbulent transition in two- and three-dimensional boundary layers. The governing Navier-Stokes equations for an incompressible fluid are:

$$\vec{U}_t + \vec{U}\cdot\nabla\vec{U} = -\nabla p + \nu\nabla^2\vec{U} + \vec{F}, \tag{1}$$

$$\nabla\cdot\vec{U} = 0, \tag{2}$$

where $\vec{U} = (u, v, w)$ is the velocity vector, p the pressure, and ν the kinematic viscosity. The term $\vec{F}$ is a forcing term to be specified later. Slip-free boundary conditions at a solid wall ($y = 0$) are imposed, i.e.,

$$\vec{U} = (x,0,z,t) = 0. \tag{3}$$

In the free stream, it is reasonable to require that

$$\vec{U} \to U_\infty \quad \text{as} \quad y \to \infty. \tag{4}$$

Equations (1-4) are solved by a Fourier-Chebyshev spectral method. Periodicity is assumed in the x and z directions. The dependent variables have Fourier-Chebyshev series of the form

$$u(x,y,z,t) = \sum_{k_x=-\frac{K_x}{2}}^{\frac{K_x}{2}-1}\sum_{k_z=-\frac{K_z}{2}}^{\frac{K_z}{2}-1}\sum_{n=0}^{N}\hat{u}(t)e^{2\pi i(k_x x/L_x)}e^{2\pi i(k_z z/L_z)}T_n(\eta) \tag{5}$$

where L_x and L_z are the periodicity lengths in x and z directions, respectively, and T_n are the Chebyshev polynomials of degree n. The spatial discretization employs spectral collocation. The collocation points for the periodic directions are

$$x_j = jL_x / K_x, \qquad j = 0,1,\ldots,K_x - 1 \tag{6}$$

$$z_m = mL_z / K_z, \qquad m = 0,1,\ldots,K_z - 1. \tag{7}$$

A staggered grid is employed in the normal direction. Velocities are defined at the points

$$\eta_q = \cos\left(\frac{\pi q}{N}\right), \qquad q = 0,1,\ldots,N \tag{8}$$

and the pressures at

$$\eta_{q+1/2} = \cos\left(\pi(q+1/2)/N\right), \qquad q = 0,1,\ldots,N-1. \tag{9}$$

No artificial pressure boundary conditions are therefore needed. The momentum equations are imposed at the points given by Eq. (8) and the continuity at those given by Eq. (9).

The normal computational coordinate η is related to y through the algebraic transformation

$$y = a\frac{1+\eta}{1+\dfrac{2a}{y_\infty} - \eta} \tag{10}$$

where a is a scaling constant used for proper distribution of points and y_∞ is the location where free stream asymptotic boundary conditions [33] are imposed.

In the spectral collocation method, spatial derivatives of u are obtained by differentiating the series expansion coefficients $\hat{u}(t)$ determined by discrete Fourier and Chebyshev transform of the grid-point values of u. The temporal discretization involves Crank-Nicolson on the pressure gradient and vertical diffusion terms. The remaining terms in the momentum equations are handled explicitly by using second-order Adams-Bashforth method. The incompressibility constraint is imposed implicitly. The resulting implicit equations are solved iteratively by a minimum residual method. The details of the procedure are given by Malik et al. [33] .

2.1 Flow over a curved wall

The numerical procedure outlined above is applicable to the study of transition problem in two- and three-dimensional boundary layers where TS, Görtler or crossflow instability mechanisms may be operative. In order to explain the numerical approach, we describe the application of the method to the flow over a concavely curved plate where both Görtler and TS waves might exist. Extension to three-dimensional boundary layers will be considered in a later section.

Consider incompressible flow with free stream velocity U_∞ along a mildly curved wall with constant curvature $\kappa = \ell / r$ where ℓ is a characteristic length scale and r is the radius of curvature of the wall. If x is the distance along the curved wall, z along the span, and y normal to the wall, then the governing equations represented in body-oriented coordinates are

$$\frac{\partial u}{\partial t} + \lambda u \frac{\partial u}{\partial x} + v \frac{\partial u}{\partial y} + w \frac{\partial u}{\partial z} + \gamma u v = -\lambda \frac{\partial p}{\partial x} + \nu \left[\nabla^2 u - \gamma^2 u + 2\gamma\lambda \frac{\partial v}{\partial x} \right], \tag{11}$$

$$\frac{\partial v}{\partial t} + \lambda u \frac{\partial v}{\partial x} + v \frac{\partial v}{\partial y} + w \frac{\partial v}{\partial z} - \gamma u^2 = -\frac{\partial p}{\partial y} + \nu \left[\nabla^2 v - \gamma^2 v - 2\gamma\lambda \frac{\partial u}{\partial x} \right], \tag{12}$$

$$\frac{\partial w}{\partial t} + \lambda u \frac{\partial w}{\partial x} + v \frac{\partial w}{\partial y} + w \frac{\partial w}{\partial z} = -\frac{\partial p}{\partial z} + \nu \nabla^2 \omega, \tag{13}$$

$$\lambda \frac{\partial u}{\partial x} + \frac{\partial v}{\partial y} + \frac{\partial w}{\partial z} + \gamma v = 0, \tag{14}$$

where

$$\nabla^2 = \lambda^2 \frac{\partial^2}{\partial x^2} + \frac{\partial^2}{\partial y^2} + \frac{\partial^2}{\partial z^2} + \gamma \frac{\partial}{\partial y}$$

$$\lambda = \frac{1}{1 + \kappa y} \quad , \quad \gamma = \frac{\kappa}{1 + \kappa y}.$$

In Eqs. (11-14), if all velocities are assumed to be scaled by U_∞, lengths by ℓ, time by ℓ/U_∞, pressure by ρU_∞^2, then $\nu = 1/R$, where R is the Reynolds number. A Görtler number can be defined as $G = R\sqrt{|\kappa|}$.

According to first-order boundary layer theory, the above equations reduce to the Blasius flow which provides the basic flow for our study of nonlinear development of Görtler vortices and Görtler/TS interaction in a two-dimensional boundary layer.

2.2 Linear Stability Theory

We consider an infinitesimally small disturbance superposed on the Blasius flow. For instance, the streamwise velocity $u(x,y,z,t)$ may be written as

$$u(x,y,z,t) = U_B(y) + \varepsilon\hat{u}(y)e^{i(\alpha x+\beta z-\omega t)} \tag{15}$$

under the quasi-parallel flow assumption. Here ε is a small parameter, α and β are disturbance wave numbers in x,z directions respectively and $\omega = \omega_r + i\omega_i$ is the complex frequency. The real part ω_r is the actual disturbance frequency and the imaginary part ω_i is the temporal growth rate. The disturbance amplitude increases if $\omega_i > 0$, otherwise the disturbance dies out.

Linear stability equations may be derived by substituting $u(x,y,z,t)$ from Equation (15) and similar expressions for other dependent variables into the Navier-Stokes equations (11-14) and then retaining only terms of $0(\varepsilon)$. The resulting sixth-order system of ordinary differential equations describes an eigenvalue problem for parameters α, β and ω which is solved by the fourth-order accurate compact difference scheme of Malik et al. [34]. Depending upon the values of Görtler number G and wave numbers (α,β), the governing equations yield solution for both the Görtler vortices and TS

waves. These solutions are needed to provide initial conditions for the non-linear calculations. In figures (1-2), we provide linear results for Görtler and TS waves to emphasize differences between the two instabilities. Description for figures (1-2) is provided below.

2.3 Nonlinear Simulations

Various nonlinear problems may now be formulated. Suppose, we are interested to study the nonlinear development of Görtler vortices. A steady Görtler vortex is characterized by $\omega_r = \alpha_r = 0,\ G > 0,\ \beta > 0$. We solve linear stability problem for Blasius boundary layer and find $\beta = \beta_G$, the growth rate ω_i and the disturbance eigenfunctions $\hat{u}_G, \hat{v}_G, \hat{w}_G$. These are presented in Figure 1. The plots show that the streamwise component $\hat{u}_G$ is an order of magnitude larger than the cross-stream components $\hat{v}_G$, and $\hat{w}_G$. The spanwise component is 90° out of phase with $\hat{u}_G$ and $\hat{v}_G$. This allows steady Görtler vortex problem to be represented as a system of real equations. In the present case, our complex system of equations automatically yields the real solution for the steady Görtler vortex. The structure of $\hat{v}_G$ and $\hat{w}_G$ is such that it results in a pair of counter-rotating vortices. Here we only consider steady Görtler vortices since in the experiments these vortices are commonly found to be steady. The Görtler vortex is assigned an initial finite-amplitude ε_G. Then an initial velocity, say for x component of velocity, is of the form

$$u(x,y,z,0) = U_B(y) + \varepsilon_G \mathrm{Real}\left[\hat{u}_G(y) e^{i\beta_G z}\right] \tag{16}$$

Equations (11-14) are solved with these initial conditions and solution is marched in time. The solution yields the development of the fundamental and various harmonics depending upon the number of modes

allowed in the simulation according to Eq. (5). The temporal development is related to the spatial development through group velocity transformation $\left(C_g = \partial\omega / \partial\alpha\right)$ as for TS waves.

The eigenfunctions for a TS wave are presented in Figure 2. The eigenfunctions are now complex with disturbance peak lying closer to the solid boundary. The interaction of a Görtler vortex with two oblique TS waves may be studied by choosing the following initial conditions:

$$u(x,y,z,0) = U_P(y) + \varepsilon_G \mathrm{Real}\left[\hat{u}_G(y)e^{i\beta_G z}\right] + \varepsilon_{TS}\left\{\mathrm{Real}\left[\hat{u}(y)e^{i(\alpha_{TS}x+\beta_{TS}z)}\right]\right.$$

$$\left.+\mathrm{Real}\left[\hat{u}(y)e^{i(\alpha_{TS}x-\beta_{TS}z)}\right]\right\} \tag{17}$$

Here various values of β_{TS} in relation to β_G may be assigned. For example, $\beta_{TS} = \beta_{G/2}$ describes a subharmonic resonance and $\beta_{TS} = \beta_{GS}$ describes a fundamental resonance. Relative magnitudes of ε_G and ε_{TS} describes various regimes of interaction where either Görtler vortex or TS wave is small or when both have large amplitude and interact nonlinearly.

How the numerical simulation may be used to study the intermodal interaction may be best described by providing the example of subharmonic instability in a flat plate boundary layer. This instability which is the result of parametric resonance between a two-dimensional TS wave and oblique TS waves with streamwise wavelength twice that of the fundamental was first theoretically studied by Herbert [5] using Floquet analysis. Here we consider the fundamental wave to have α = .2033 and prescribe R = 606. An amplitude of .01 (i.e., 1%) is assigned to the two-dimensional TS wave.

According to Herbert, a strong subharmonic instability of wave numbers $((\alpha/2), \beta)$ should develop for a wide range of β, (see Fig. 9 in [5]). The present calculation is performed by including in the initial conditions

two oblique modes ($\alpha/2$, β = ± .16968). Results of the calculation are presented in Fig. 3. In this figure, the natural logarithm of the energy history of the modes (α,0) and ($\alpha/2$, β) are plotted as a function of time. Calculations are carried out to about 3.5 linear time periods of the finite-amplitude two-dimensional wave. The solid curves are the linear theory results for the corresponding modes. The finite-amplitude two-dimensional wave follows its linear growth (ω_i = .7E-5) curve within the computational domain. The subharmonic ($\alpha/2$, β) follows the linear theory result for primary subharmonic for some time and then diverges from it indicating strong secondary instability. The growth rate at the onset of this instability is $\omega_i \approx$ .0098 which drops to $\omega_i \approx$ .0071 towards the end of the computation due to nonlinear effects. This is in good agreement with the prediction of Herbert for ω_i = .00824. The subharmonic secondary instability has been linked to the squire mode by Herbert. However, in order to capture the instability using numerical simulations, we need not provide the actual eigenfunctions for the squire mode in the initial conditions. In our calculations we have used the eigenfunctions for the primary subharmonic. In another calculation the initial conditions for the ($\alpha/2,\pm\beta$) modes were arbitrarily taken to be

$$\hat{u} = 0, \qquad \hat{v} = y^2 e^{-2(y-1)} \quad , \quad \text{and} \quad \hat{w} = \pm \frac{i}{\beta} \frac{\partial \hat{v}}{\partial y} \tag{18}$$

The results are presented in Figure 4. Again the subharmonic secondary instability emerges. Most interestingly, both calculations converge towards the same growth rate for the subharmonic. Higher harmonics also grow in these nonlinear calculations. In a transition simulation, one would like to assign a small random distribution of energy to all the modes, except, of

course, the finite-amplitude disturbance and let the dominant pattern evolve by itself.

In our calculations we allow the mean flow to develop in time in order to simulate the development of Blasius profile along the curved plate. This is achieved by specifying the forcing term F in Eq. (1) as

$$F = -\nu \frac{\partial^2 U_B}{\partial y^2} + \frac{\partial U_B}{\partial t} \tag{19}$$

where

$$\frac{\partial U_B}{\partial t} = C_g \frac{\partial U_B}{\partial x}$$

with C_g being the disturbance group velocity defined above.

3. NONLINEAR DEVELOPMENT OF GORTLER VORTICES

Before embarking upon a study of Görtler/Tollmien-Schlichting wave interaction, it is important to study the nonlinear development of Görtler vortices to demonstrate that our numerical model adequately describes the phenomenon of interest. This we attempt to achieve by performing calculations for the conditions of the experiment of Swearingen and Blackwelder [14]. The experiment of Swearingen and Blackwelder was performed in a low speed wind tunnel specially designed to have a concave wall in order to study Görtler instability. The radius of curvature of the wall was r = 3.2 m. Our calculations start at x = 45 cm which, for a free stream speed of 5 m/s, gives an $R = \sqrt{\mathrm{Re}_x}$ = 395 and a Görtler number G = 7.5. The initial amplitude for the Görtler vortex is taken to be 5%. The effective Görtler number increases as the flow is allowed to develop according to Eq. (19). The convection velocity C_g is taken to be the disturbance group velocity which is also used to transform our temporal results to spatial results for comparison with the experimental findings.

The v-w velocity vector plots are presented in Figure 5 at computational times of 181 and 880, the latter time being quite far into the nonlinear regime. The two plots are similar and indicate the counter-rotating structure of the Görtler vortex except that the disturbance intensity increases and the vortices reach out further away from the wall at larger time. Two regions in these figures may be noted: one where the velocity vectors are pointed upwards away from the wall and the other where they are pointed downwards to the wall. The former will result in a low streamwise velocity region while the latter will result in a high velocity region as discussed below. These regions may be identified as "peak" and "valley" following the nomenclature of Klebanoff et al. [1] for flat plate boundary layer transition.

The distribution of the disturbance u velocity at various times (distances) is plotted in Figure 6. The solid lines represent positive velocity and the dotted lines negative velocity. Initially the two regions of positive and negative disturbance velocity look similar. As the Görtler vortex develops, the region of positive disturbance velocity gets flattened and squashed near the wall while the region of negative velocity gets elongated in a direction normal to the wall and as a result will influence the flow further away from the wall as we note in the next figure.

Figure 7 contains a comparison of the constant u (total) velocity contours at various streamwise distances. The computed results are presented in Figure 7(a) which show the development of mushroom like structure. The "mushrooms" are caused by the ejection of the low velocity fluid, away from the surface, in the "peak" region noted above. Two peaks then contain a "valley" in between as evident from the figure. This valley is caused by the movement of high velocity fluid towards the wall. The experimental results for the constant u velocity contours are given in Figure 7(b)

and also show the development of mushroom like structure. These mushrooms, which are essentially the nonlinear manifestation of the Görtler vortex, extend out of the mean Blasius boundary layer both in the experiment and the present computations.

The wall-shear stress along the peaks and valleys develop differently as shown in Figure 8 where comparison is made again with the experiment of Swearingen and Blackwelder. In the nonlinear regime, the wall shear stress continues to decrease in the "peak" region due to inflected velocity profiles while it increases along the valley due to the presence of high velocity fluid near the wall. The computed results would be valid only up to about x = 90 cm, since three dimensional effects and unsteadiness caused due to secondary instability must begin to appear which are not accounted for in the present computation. These computations do show that the early nonlinear stage is properly captured. A full 3-D calculation will be able to capture the secondary instability stage and beyond. The 3-D version of the code has been used in the Görtler/TS wave-interaction simulation and will be discussed below.

Due to the inflected velocity profiles in the "peak" region, the boundary layer considerably thickens while it thins in the "valley" region due to fuller profiles. This is depicted in Figure 9 where the computed boundary layer displacement thickness is compared with the experiment. Again, a good agreement with the experiment is found up to about x = 90 cm.

The distribution of the computed rms amplitude of velocity distribution due to Görtler vortex is compared with the experiment in Figure 10(a). Both the experiment and the computations show that the Görtler vortex reaches a saturated state. At this stage strong secondary instabilities would develop which can be studied by using our numerical model. We

expect to observe at least two types of breakdown: one involving a wavy vortex structure prior to transition while the other involving a horse-shoe type structure. The conditions for the appearance of these two structures may be established by performing numerical computations. Figure 10(b) gives the disturbance energy content in various modes. The calculation shows that, even though the higher harmonics grow rapidly, most of the energy remains in the fundamental mode. The emergence of the superharmonic ((0,2) mode) is in agreement with the experimental observation of Aihara & Koyama [15].

4. GORTLER/TOLLMIEN-SCHLICHTING WAVE INTERACTIONS

The problem of excitation of a Tollmien-Schlichting wave in the presence of a Görtler vortex is studied now. We take the initial amplitude of the Görtler vortex to be 10 percent. The non-dimensional spanwise wave number is 0.4 and the Görtler number is taken as 12. Here, we use our numerical model to investigate possible excitation of a two-dimensional (α,0) TS wave in the flow field modulated by the presence of Görtler vortices. The TS wave is an upper branch mode and has R = 600, α = .2 and the linear theory eigenvalue is (.0738, .0002). The results are presented in Figure 11 where (0,1) mode indicates the Görtler vortex and (1,0) mode the TS wave. The presence of Görtler vortex causes the growth rate of the two-dimensional TS wave to increase above its linear theory value. Towards the end of the computational domain, the growth rate of the TS wave is higher than the linear growth rate of the primary (Görtler) instability.

The eigenfunctions of the Görtler (0,1) mode are presented in Figure 12(a) for various simulation times. One characteristic that is immediately evident is that the shape of the eigenfunction remains essentially the same

for quite high amplitudes. This was confirmed by restarting the calculations for low initial amplitudes. This implies that the shape function assumption would be applicable in a secondary instability analysis for the Görtler vortex problem. At later times, however, the shape beings to change and a plateau appears in the eigenfunction distribution near the edge of the boundary layer.

The eigenfunction for the TS (1,0) mode are given in Figure 12(b). Initially, only the inner peak increases in amplitude while it moves slightly outwards from the wall. However, at later times the inner peak moves towards the wall while increasing in amplitude. After some time, the outer peak also increases in amplitude and becomes fairly broad. The appearance of this our structure is perhaps related to the broadening of Görtler vortex structure noted in Figure 12(a). Due to the presence of the Görtler vortex the mean flow is modulated and develops "wake-like" profiles which would then be subject to instabilities found in laminar wakes.

Some additional calculations were performed for a Görtler number of 14, β = 0.5 and the initial Görtler vortex amplitude of 10 percent. The TS wave is again α = .2; however, this wave decays linearly for R = 950 which is used for the results presented in Figure 13. Again the (1,0) mode grows in the presence of the Görtler vortex. Also shown in the figure are the computed growth history of the oblique (1,1) mode. Some numerical tests indicated that this mode does not get excited in the absence of (1,0) mode. However, this mode now grows due to nonlinear interaction of (0,1) and (1,0) modes.

Some calculations were also performed at the TS wave number α which corresponded to the lower branch mode. Though more tests need to be performed, it appears that the upper branch TS modes are excited while

the lower branch modes are relatively insensitive to the presence of the Görtler vortex. Although the TS waves are excited in the presence of the Görtler vortex the amplitude of the Görtler vortex required for the interaction is quite high and is at least of the order of 10 percent. Therefore, the Görtler vortices will dominate the transition process and the role of the TS waves will be only in the secondary instability stage. However, here we have only considered the case where Görtler vortices are finite-amplitude but TS waves are small. The amplitude required for TS waves to breakdown is much lower than noted above for Görtler vortices. Thus the situation will be quite different when TS waves are of finite amplitude or when both are of finite amplitude. These regimes of interaction may turn out to be much more dangerous. It may also be noted that the presence of Görtler vortices may provide the spanwise scales for internalization of free stream disturbances thus enhancing the receptivity process.

5. NONLINEAR DEVELOPMENT OF A CROSSFLOW VORTEX

The above methodology used for nonlinear simulation of Görtler vortex problem equally applies to flows with three-dimensional basic states, such as swept-wing flows and flow due to a rotating disk. The appropriate basic flow and initial conditions, however, need to be specified. The objective here is to carry out such a calculation for a swept-wing configuration and see if there are any differences between the nonlinear development of a crossflow vortex in rotating disk and swept wing flow. The former is generally used as a prototype for studying the instabilities in the swept wing flows. The secondary instability analysis of Reed [27] for a swept wing suggests that there is a resonance set up between the crossflow vortex and its superharmonic while the computational results of Malik [28] for a rotat-

ing disk do not suggest any such resonance. It is therefore important to investigate any differences that might exist between the two flows.

5.1 Rotating Disk Boundary Layer

We first review the results which have been obtained for rotating disk flow. Just like the swept-wing flow, this boundary layer is amendable to inflectional instability which manifests itself in the form of stationary co-rotating vortices known as crossflow vortices since they are caused by the instability of the crossflow velocity profiles. An exact steady solution to the Navier-Stokes equations exists for rotating disk flow and this is one of the reasons why this flow has quite often been used as a prototype for studying instability mechanism in the swept wing flow. The mean flow for the rotating disk is governed by the ordinary differential (von Karman [35]) equations:

$$F^2 - (G+1)^2 + F'H - F'' = 0, \tag{20}$$

$$2F(G+1) + G'H - G'' = 0, \tag{21}$$

$$\Pi' + HH' - H'' = 0, \tag{22}$$

$$2F + H' = 0, \tag{23}$$

where F, G, H and Π are related to the velocity components and pressure according to

$$\begin{aligned} V_r &= r\Omega F(y), \qquad V_\theta = r\Omega G(y), \\ V_y &= \sqrt{\nu\Omega}H(y), \qquad P = \rho\Omega\nu\Pi(y). \end{aligned} \tag{24}$$

where Ω is the angular speed of the disk. The above equations are solved subject to the boundary conditions

$$F = 0,\ G = 0,\ H = 0,\ y = 0 \tag{25}$$

$$F = 0,\ G = -1,\ y \to \infty \tag{26}$$

A nonlinear calculation was initiated by imposing a disturbance upon the three-dimensional basic state computed above. The disturbance shape was taken to be that given by the linear eigenfunction which was assigned an amplitude of 10 percent with respect to the mean flow. The wave numbers in the radial and azimuthal directions are α = .3751 and β = .0777 which may be labelled as (1,1) mode. The results for the energies of (1,1), (2,2), (3,3), (4,4) and (5,5) modes are presented in Figure 14. The solid curve represents the linear theory result for the (1,1) mode. Spectral broadening takes place and the super-harmonics gain energy as the growth of the fundamental slows down. The energy cascading takes place through (2,2), (3,3), (4,4), etc. modes. All the modes tend to saturate and the harmonics do not overtake the fundamental mode.

The azimuthal velocity profiles at fixed radius but at various azimuthal locations within the computational domain are presented in Figure 15. The nondimensional time of the simulation is 170. While the von Karman profile is full with no inflection point, the computed flow develops "wake-like" profiles at y around 2.5. These profiles are amenable to secondary instabilities. However, no attempt was made here to capture these instabilities.

Hot-wire traces at various radii from the experiment of Wilkinson and Malik [22] are presented in Figure 16(a). The hot-wire is located at y = 1.8 and is oriented such that it essentially senses the perturbations in the azimuthal velocity component. The traces develop a "kink" which may be attributed to the superharmonic. The computational traces at various radii are presented in Figure 16(b). The nondimensional time of the simu-

lation is again 170. The computational trace appears to develop the same type of "kink" as in the experiment. The amplitude of this "kink", apparently caused by the superharmonic, is small compared to the fundamental both in the computation and the experiment. The superharmonic appears due to the self-interaction of the crossflow vortex.

5.2 Falkner-Skan-Cooke Boundary Layer

Basic insight into instability of flow past a swept wing may be achieved by considering Falkner-Skan-Cooke (FSC) flow. To this end, let us consider boundary layer flow over an infinite swept wedge at zero incidence. The governing equations may be written as (see Rosenhead [36])

$$f''' + ff'' + \bar{\beta}(1 - f'') = 0 \tag{27}$$

$$g'' + fg' = 0 \tag{28}$$

where $u / u_e = f'(\eta)$, $w / w_e = g(\eta)$ (u_e and w_e being the boundary layer edge velocities in the chordwise x and spanwise z directions (see Figure 17) respectively), and $\bar{\beta}$ is the Hartree pressure gradient parameter. The similarity parameter η is defined as

$$\eta = \sqrt{\frac{u_e}{(2-\bar{\beta})\nu x}}\; y \tag{29}$$

The above equations are to be solved subject to the boundary conditions:

$$f = f' = g = 0 \quad ; \quad \eta = 0 \tag{30}$$

$$f' \to 1, \quad g \to 1 \quad ; \quad \eta \to \infty \tag{31}$$

With reference to Figure 17, the streamwise and crossflow velocity profiles can be constructed for FSC flow as

$$U(y) = f'(y)\cos^2\theta + g(y)\sin^2\theta \tag{32}$$

$$W(y) = [-f'(y) + g(y)]\sin\theta\cos\theta \tag{33}$$

where both the streamwise and crossflow velocities, U and W in x_s and z_s directions respectively, have been scaled with $V_e = \sqrt{u_e^2 + w_e^2}$ and the external streamline angle θ is given as

$$\theta = \tan^{-1}\left(\frac{w_e}{u_e}\right) \tag{34}$$

The functions U and W for $\overline{\beta} = 0.6$ are ploltted in Figure 18 where y is the nondimensional distance normal to the surface and has been scaled with $\ell = \sqrt{\nu x / u_e}$.

In Figure 17, x_v is along the axis of the crossflow vortex which is oriented at some small angle ϕ with the free stream direction. The vortex coordinate system (x_v, y, z_v) is used for the nonlinear simulation of the crossflow vortex. The analysis begins by imposing a disturbance of the form

$$\tilde{u}(x_v, y, z_v, t) = \hat{u}(y)e^{i(\beta_v z_v - \alpha t)} \tag{35}$$

on the FSC flow. The wave front is then aligned with x_v direction. Here we consider a stationary disturbance so that Real (ω) = 0 and Im(ω) corresponds to the temporal growth rate of the vortex. The calculations are performed for the following conditions:

$$R = V_e \ell / \nu = 800$$

and

$$\beta_v = 0.48, \quad \phi = -4.135°.$$

The above combination of parameters results in a stationary vortex (ω_r = 0) disturbance according to linear theory. The linear theory growth rate is .0065. The crossflow Reynolds number is 244.

Linear eigenfunctions were first obtained to provide initial conditions for the nonlinear simulations. The eigenfunctions $\hat{u}, \hat{v}, \hat{w}$ are plotted in

Figure 19. These can be compared with the results presented in Figure 1 for Görtler vortex which is also a stationary streamwise vortex. We note that the eigenfunctions are complex for the crossflow vortex; however, just like the Görtler vortex the magnitudes of $\hat{v}$,$\hat{w}$ components are much smaller than the $\hat{u}$ component along the axis of the stationary crossflow vortex.

These eigenfunctions were included in the initial conditions for the numerical study of the nonlinear evolution of the crossflow vortex. The initial amplitude was taken to be 5 percent. The (v,w) vector plots are presented in Figure 20. As opposed to the vector plots given in Figure 5 for the Görtler vortex, it can be seen that crossflow vortices are corotating vortices with one vortex per wave length. The disturbance intensity increases as the vortices develop nonlinearly (compare Figures 20(a) and (c)).

The evolution of the energies of various modes is given in Figure 21. Just like in the case of a Görtler vortex, higher harmonics grow and they all tend to saturate. The energy in the fundamental (0,1) mode dominates. This is quite similar to what was observed above for a crossflow vortex in rotating disk flow.

Saric & Yeates [26] observed that, in addition to the fundamental wavelength, an additional peak in the hot-wire trace appears at some height from the wall with half the wavelength. This latter peak had an amplitude about 3 times that of the fundamental. The surface flow visualizations only showed streaks at the wavelength given by the fundamental. Reed [27] attempted to explain the anomaly found in the experiment by using secondary instability theory based upon Floquet analysis. Thus the periodic basic flow was constructed by superposing on the three-dimensional boundary layer the eigenfunctions for the crossflow vortex of

wavenumber β_v. The amplitude assigned to this disturbance was 7 percent in order to simulate the experimental conditions. Linear instability analysis of this basic flow revealed that a disturbance of wavenumber $2\beta_v$ is amplified while this disturbance is stable from a linear analysis of the boundary layer flow alone. However, the growth rate for the superharmonic $2\beta_v$ was found to be almost the same as for the fundamental β_v mode and, thus, one of the basic assumptions of the secondary instability theory was violated. In any case, the eigenfunctions obtained from the secondary instability analysis were assigned an amplitude of 21 percent (3 times the fundamental) and the streamlines for the resulting flow were constructed which showed two vortices per wavelength of the fundamental instability. The results appeared to explain the observations of Saric and Yeates [26]. However, we note that in our nonlinear calculations presented in Figure 21, the superharmonic does not achieve amplitude higher than that of the fundamental, let alone three times the amplitude of the fundamental.

It may well be that the superharmonic has an eigenfunction structure which has local peak somewhere in the boundary layer at an amplitude of about 3 times that of the fundamental as observed in the experiment of Saric and Yeates. Therefore, we plot the eigenfunctions for the fundamental and the superharmonic at four different times in Figure 22. The $\hat{u}$ amplitude of the fundamental and the superharmonic increases with time but no where in the boundary layer the latter attains amplitude higher than that of the former.

The fundamental $\hat{u}$ perturbation eigenfunction develops a "kink" which at later times develops into a double peak. Somewhat similar structure appears in the swept wing experiments of Dagenhart et al. [25] but is unsteady. At this time, we have not attempted to find the frequency content

of the computed signal. Such a comparison will be meaningful when the calculations are performed for the exact conditions of the experiment of Dagenhart et al. We also note that initially the shape of the fundamental eigenfunction is preserved even though the amplitude is relatively large. This lends some support to the shape function assumption generally used in the secondary instability analysis.

The computational traces of u at various heights in the boundary layer and at three different times are presented in Fig. 23. The $u(z_v)$ velocity develops a "kink" similar to that found for the rotating disk case due to the development of the superharmonic. This kink is quite pronounced at a certain height from the surface. A hot-wire traversed in the spanwise direction at this particular height will indicate the presence of a disturbance with half the wavelength of the fundamental; however, as noted above the amplitude of the superharmonic is less than the fundamental. The observation of Saric & Yeates that the superharmonic attains three time the amplitude of the fundamental may be the result of certain conditions unique to the experiment, particularly when the experiments of Müller & Bippes [24] and Dagenhart et al. [25] fail to observe the phenomenon noted by Saric & Yeates. It may be that the nonparallel/ nonlinear calculations for the exact conditions of the Saric-Yeates experiment will explain the observed results. Nonparallel effects are accounted for neither in the secondary instability analysis of Reed [27] nor in the present temporal numerical simulations. In any case, we conclude that the anomaly found in the Saric-Yeates experiment, namely that the superharmonic attains an amplitude three times that of fundamental, remains unexplained.

The velocity profiles parallel and at 90° to the crossflow vortex axis at various spanwise locations are presented in Figure 24. Again, inflected "wake-like" profiles develop in the direction of the vortex axis (which is at an angle of -4.135° with respect to the inviscid streamline) due to nonlinear distortion of the crossflow vortex as also found for the rotating disk. These profiles will be subject to inviscid secondary instability. From the results presented in this section, it becomes quite clear that the nonlinear development of a crossflow vortex in FSC boundary layer is quite similar to what was found for a rotating disk.

5.3 Secondary Instability in FSC Boundary Layer

The computed Falkner-Skan-Cooke flow field in the presence of a crossflow vortex has been presented above. It is of interest to investigate the type of secondary instabilities this flow may be subjected to. The present numerical simulations have been used to investigate one such instability. The calculations have been performed for the parameter values used above in the nonlinear simulation of the crossflow vortex. However, included in the initial conditions is a mode with $\alpha_v = 0.48$ and $\beta_v = 0.48$. This unsteady mode is highly damped according to the linear theory. The growth rate of this mode computed from our numerical simulations is plotted in Figure 25. Initially, the mode is damped, in agreement with the linear stability theory. However, after about $t = 100$, this mode begins to grow. The growth rate distribution is oscillatory because of the interactions with other modes, but eventually the growth rate of this mode is much larger than the linear growth rate of the crossflow vortex ((0,1) mode) indicated by circles in the figure. The computed growth rate of the (0,1) mode indicated by a dashed line is also shown and it approaches zero as the crossflow mode saturates.

The (α_v,β_v) mode (denoted as (1,1) mode) thus develops quite quickly and will perhaps provide at least one mechanism for breakdown of the crossflow vortex. The values of α_v and β_v chosen here imply a wave oriented at an angle of about 45° with respect to the crossflow vortex.

For rotating disk flow, Kohama [37] observed that prior to transition a new instability, in the form of small vortices, appears on the surface of crossflow vortices. These vortices were oriented at an angle of about 45° with respect to the crossflow vortex. The structure observed by Kohama is, perhaps, the result of a localized instability which takes place at some distance away from the wall and produces an illusion of the "vortices" riding on the crossflow vortex. Obviously, the flow visualization technique used can not provide the true nature of the instability. In any case, it appears that the secondary instability computed here may provide a clue for the explanation of the experiment of Kohama. It, therefore, would be desirable to further investigate this phenomenon using Floquet analysis and more numerical simulations. It may be noted here that since the growth rate of the (α_v,β_v) mode is about 4-5 times the linear growth rate of the crossflow vortex ($(0,\beta_v)$ mode), Floquet analysis can provide useful results. Further investigations into the nature of this secondary instability will be made at a later date.

6. CONCLUSIONS

We have used direct numerical simulations to investigate nonlinear development of Görtler and crossflow vortices and to study Görtler/TS wave interactions. Our results show that when Görtler vortex develops nonlinearly, higher harmonics grow but most of the energy remains in the fundamental mode. The flow field in the presence of the nonlinear Görtler

vortex has been computed for the conditions of the experiment of Swearingen & Blackwelder [14]. In agreement with the experiment, a "mushroom" like structure appears as the low velocity fluid is ejected upwards between the counter-rotating Görtler vortices. In this "peak" region, wall shear stress decreases while the displacement thickness increases relative to the mean Blasius boundary layer. The converse is true for the "valley" region where the high velocity fluid is pushed towards the wall.

Numerical simulations are also used to study the excitation of a two-dimensional TS wave in the presence of a finite-amplitude Görtler vortex. The results indicate that the TS wave grows faster than its linear growth rate and that oblique TS waves also grow due to nonlinear interactions. These oblique waves are linearly stable. The amplitude of the Görtler vortex at which the interaction takes place are much larger than that needed in flows where *finite-amplitude* TS waves *constitute* the primary instability.

Finally, we have used the computational approach to simulate the nonlinear development of a crossflow vortex in a Falkner-Skan-Cooke boundary layer. It is shown that nonlinear development of a crossflow vortex in FSC and rotating disk boundary layer are similar. In both flows, the fundamental saturates at sufficiently large amplitudes along with the harmonics. The first superharmonic clearly emerges in the velocity signal but its amplitude remains smaller than the fundamental. A new type of secondary instability is noted in the numerical simulations. This instability is found to have growth rates which are 4 to 5 times higher than the growth rate of the linear crossflow vortex.

REFERENCES

1. Klebanoff, P. S., Tidstrom, K. D., and Sargent, L. M., "The Three-Dimensional Nature of Boundary-Layer Instability," J. Fluid Mech., Vol. 12, 1962, pp. 1-34.

2. Kachanov, Y. S., "On the Resonant Nature of the Breakdown of a Laminar Boundary Layer," J. Fluid Mech., Vol. 184, 1987, pp. 43-74.

3. Saric, W. S. and Thomas, A. S. W., "Experiments on the Subharmonic Route to Turbulence in Boundary Layers," in Turbulence and Chaotic Phenomena in Fluids (ed. T. Tatsumi), 117-122, North-Holland, 1984.

4. Craik, A. D. D., "Non-linear Resonant Instability in Boundary Layers," J. Fluid Mech., Vol. 50, 1971, pp. 393-412.

5. Herbert, T., "Secondary Instability of Boundary Layers," Ann. Rev. Fluid Mech., Vol. 20, 1988, pp. 487-526.

6. Wray, A. and Hussaini, M. Y., "Numerical Experiments in Boundary Layer Stability," Proc. Roy. Soc. Lond. A, Vol. 392, 1984, pp. 373-389.

7. Orszag, S. A. and Patera, A. T., "Secondary Instability of Wall-Bounded Shear Flows," Journal of Fluid Mechanics, Vol. 128, pp. 1983, 347-385.

8. Spalart, P. R. and Yang, K. S., "Numerical Simulation of Ribbon-Induced Transition in Blasius Flow," J. Fluid Mech., Vol. 178, 1987, pp. 345-365.

9. Laurien, E. and Kleiser, L., "Numerical Simulation of Boundary-Layer Transition and Transition Control," J. Fluid Mech., Vol. 199, 1989, pp. 403-440.

10. Zang, T. A. and Hussaini, M. Y., "Numerical Experiments on Subcritical Transition Mechanisms," AIAA Paper No. 85-0296, 1985a.

11. Fasel, H. F., Rist, U., and Konzelmann, U., "Numerical Investigation of the Three-Dimensional Development in Boundary-Layer Transition," AIAA Paper No. 87-1203, 1987.

12. Bippes. H. and Görtler, H., "Dreidimensionales Störunge in der Grenzschicht an Einer Konkaven Wand," Aera. Mech., Vol. 14, 1972, pp. 251-267.

13. Winoto, S. H. and Crane, R. I., "Vortex Structure in Laminar Boundary Layers on a Concave Wall," Int. J. Heat and Flux Flow, Vol. 2, 1980, pp. 221.

14. Swearingen, J. D. and Blackwelder, R. F., "The Growth and Breakdown of Streamwise Vortices in the Presence of a Wall," J. Fluid Mech., Vol. 182, pp. 255-290.

15. Aihara, Y. and Koyama, H., "Secondary Instability of Görtler Vortices: Formation of Periodic Three-Dimensional Coherent Structures," Trans. Japan Soc. Aero. Space Sci., Vol. 24, 1981, pp. 78-94.

16. Bippes, H., "Experimental Study of the Laminar-Turbulent Transition of a Concave Wall in a Parallel Flow," NASA TM-75243, 1978.

17. Jeans, A. H. and Johnston, J. B., "The Effect of Streamwise Concave Curvature on Turbulent Boundary Layer Structure," Stanford Report MD 40, Thermosciences Division, Department of Mechanical Engineering, Stanford University 1983.

18. Gray, W. E., "The Nature of the Boundary Layer Flow at the Nose of a Swept Wing," Royal Aeronautical Establishment, Tech. Memo. (Aero) 256, June 1952.

19. Owen, P. R. and Randall, D. G., "Boundary Layer Transition on a Swept Back Wing," Royal Aircraft Establishment, Tech. Memo. (Aero) 256, Feb. 1952.

20. Gregory, N., Stuart, J. T., and Walker, W. S., "On the Stability of Three-Dimensional Boundary Layers with Application to the Flow Due to a Rotating Disk," Phil. Trans. Roy. Soc. A, Vol. 248, 1955, pp. 155-199.

21. Smith, N. H., "Exploratory Investigation of Laminar Boundary Layer Oscillations on a Rotating Disk," Phil. Trans. Roy. Soc. Lond., A, Vol. 248, 1955, pp. 155-199.

22. Wilkinson, S. P. and Malik, M. R., "Stability Experiments in the Flow over a Rotating Disk," AIAA Journal, Vol. 23, 1985, p. 588.

23. Malik, M. R. and Poll, D. I. A., "Effect of Curvature on Three-Dimensional Boundary Layer Stability," AIAA Journal, Vol. 23, pp. 1362-1369.

24. Müller, B. and Bippes, H., "Experimental Study of Instability Modes in a Three-Dimensional Boundary Layer," AGARD-CP- 438, Paper No. 13, October 1988, pp. 13-1 -13-15.

25. Dagenhart, J. R., Saric, W. S., Mousseaux, M. C. and Stack, J. P., "Crossflow Vortex Instability and Transition on a 45-Degree Swept Wing," AIAA Paper No. 89-1892, 1989.

26. Saric, W. S. and Yeates, L. G., "Generation of Crossflow Vortices in a Three-Dimensional Flat-Plate Flow," IUTAM Symp. on Laminar-Turbulent Transition, Novosibirsk, U.S.S.R., July 9-13, 1984, Springer, Verlag.

27. Reed, H. L., "Wave Interactions in Swept-Wing Flows," Physics of Fluids, Vol. 30, No. 11, Nov. 1987, pp. 3419-3426.

28. Malik, M. R., "Numerical Simulation of Transition in a Three-Dimensional Boundary Layer," in Proceedings of the Tenth International Conference on Numerical Methods in Fluid Dynamics, June 23-27, 1986, Beijing, pp. 455-461.

29. Meyer, F. and Kleiser, L., "Numerical Investigation of Transition in 3D Boundary Layers," presented at the AGARD Symposium on Fluid Dynamics of Three-Dimensional Turbulent Shear Flows and Transition, Cesme, Turkey, October 3-6, 1988.

30. Malik, M. R., "Wave-Interactions in Three-Dimensional Boundary Layers," AIAA Paper No. 86-1129.

31. Hall, P. and Smith, F. T., "The Nonlinear Interaction of Tollmien-Schlichting Waves and Taylor-Görtler Vortices in Curved Channel Flows," NASA CR-178283, 1987.

32. Nayfeh, A. H. and Al-Maaitah, A., "Influence of Streamwise Vortices on Tollmien-Schlichting Waves," Phys. Fluids, Vol. 31, No. 12, 1988, pp. 3543-3549.

33. Malik, M. R., Zang, T. A., and Hussaini, M. Y., "A Spectral Collocation Method for the Navier-Stokes Equations," Journal of Computational Physics, Vol. 61, 1985, pp. 64-88.

34. Malik, M. R., Chuang, S., and Hussaini, M. Y., "Accurate Numerical Solution of Compressible Stability Equations," ZAMP, Vol. 33, 1982, pp. 189-201.

35. von Karman, T., "Uber Laminare und Turbulente Reibung," Zeitschrift für Angewande Mathematik und Mechanik, Vol. 20, 1940, pp. 241-253.

36. Rosenhead, L., Laminar Boundary Layers, Oxford University Press, 1963.

37. Kohama, Y., "Coherent Structures in Three-Dimensional Boundary-Layer Transition," in Proc. of the Third Asian Congress of Fluid Mechanics, September 1-5, 1986, Tokyo, pp. 162-165.

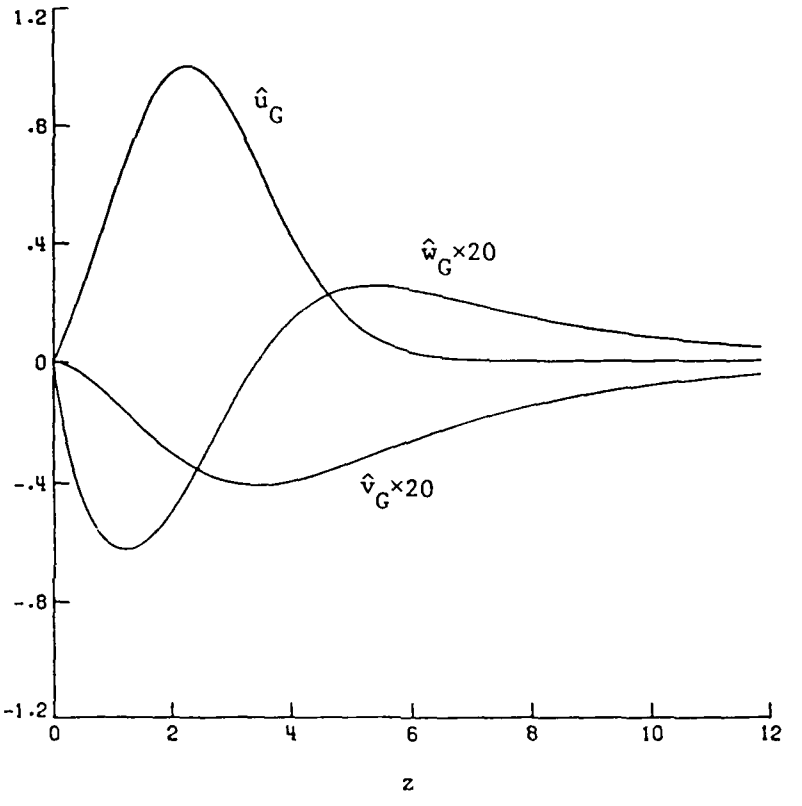

Figure 1. Eigenfunctions for a Görtler vortex in a Blasius boundary layer, $G = 14$, $\beta = .3$.

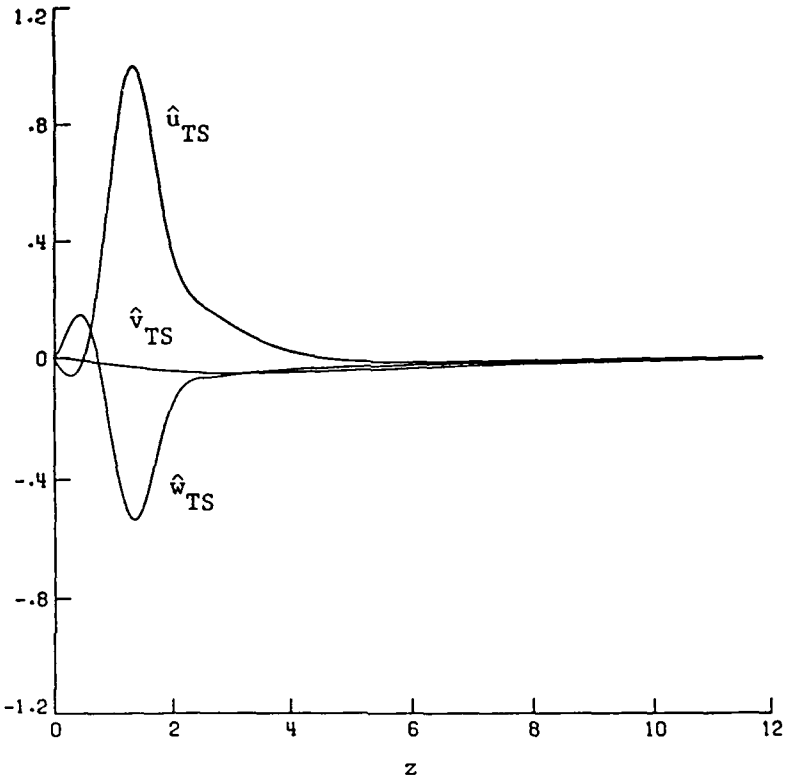

(a) real part

Figure 2. Eigenfunctions for an oblique TS wave in a Blasius boundary layer, $R = 950$, $\alpha = .103$, $\beta = .15$.

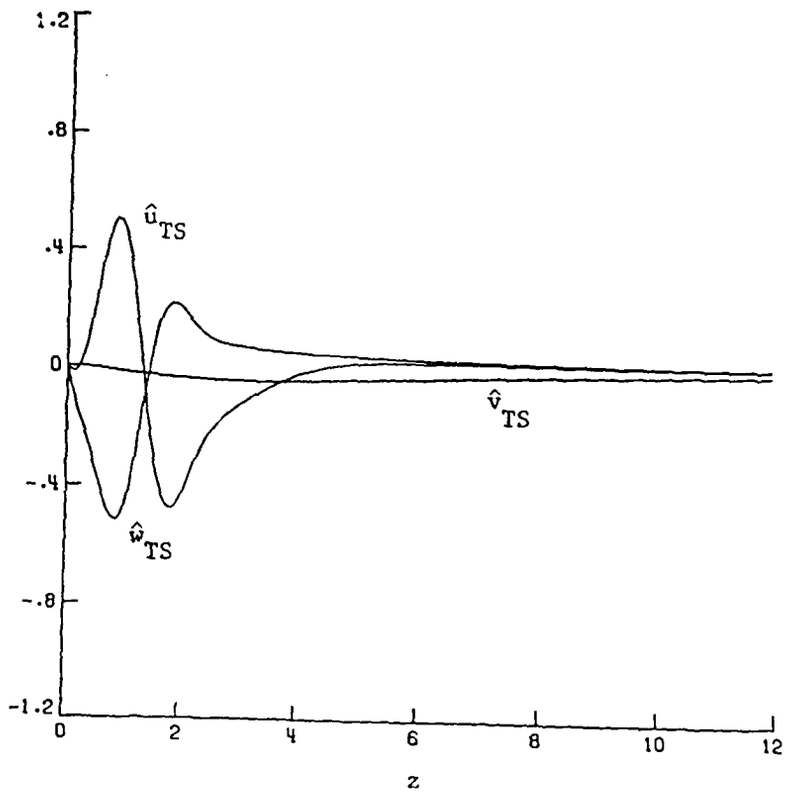

(b) imaginary part

Figure 2. Concluded.

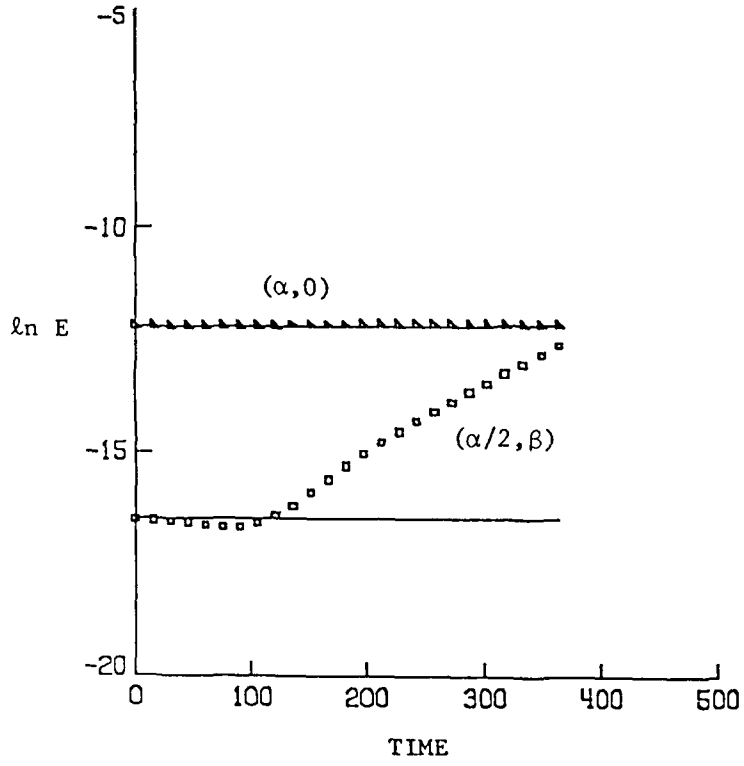

Figure 3. Computed evolution of energies of a two-dimensional TS wave ($(\alpha,0)$ mode) and the oblique subharmonic ($(\alpha/2,\beta$ mode). In this calculation, R = 606, α = .2033, β = .16968. A strong secondary subharmonic instability develops. Included in the initial conditions are two oblique primary subharmonics. The solid lines represent linear theory results.

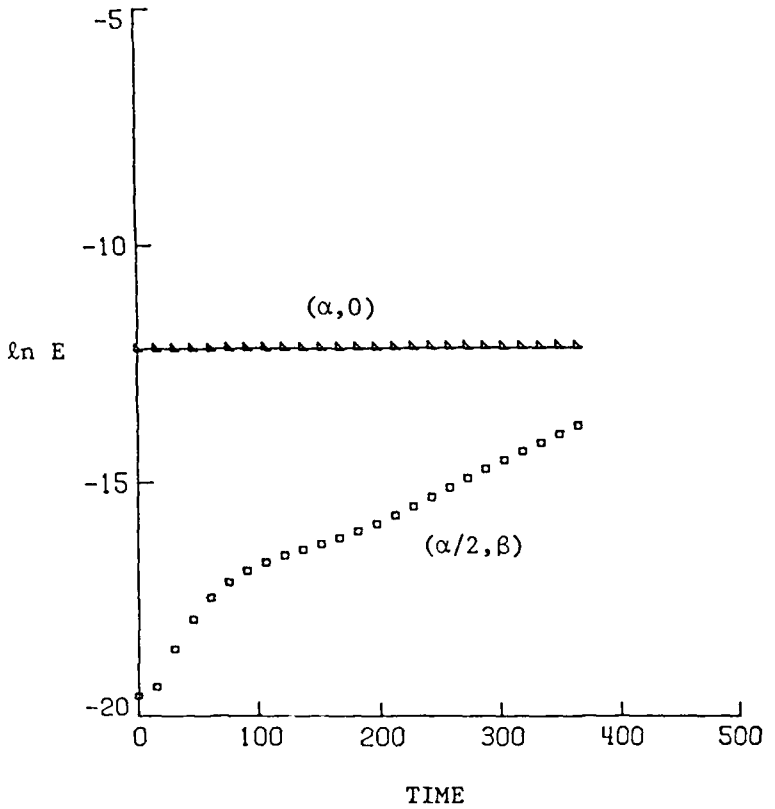

Figure 4. Same as for Figure 3 except the initial conditions for the subharmonic were those given in Eq. (18).

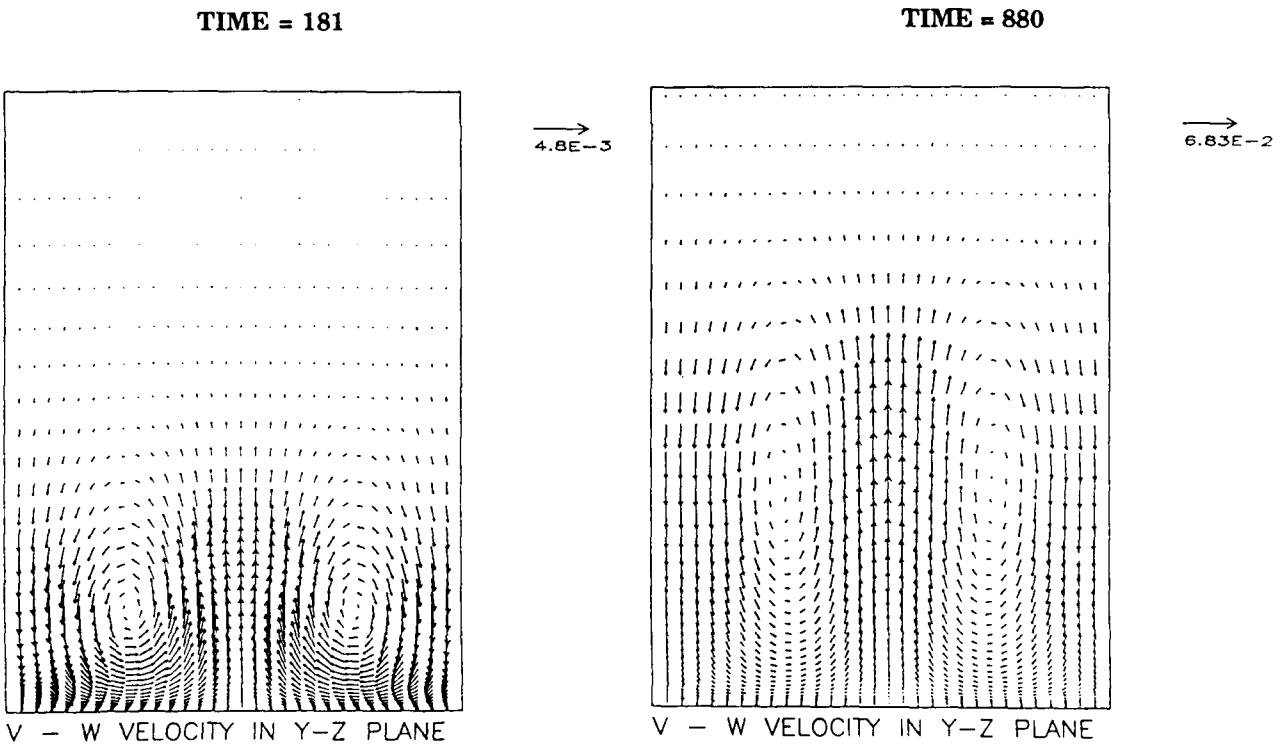

Figure 5. Velocity vector plot in y-z plane for Görtler vortex flow.

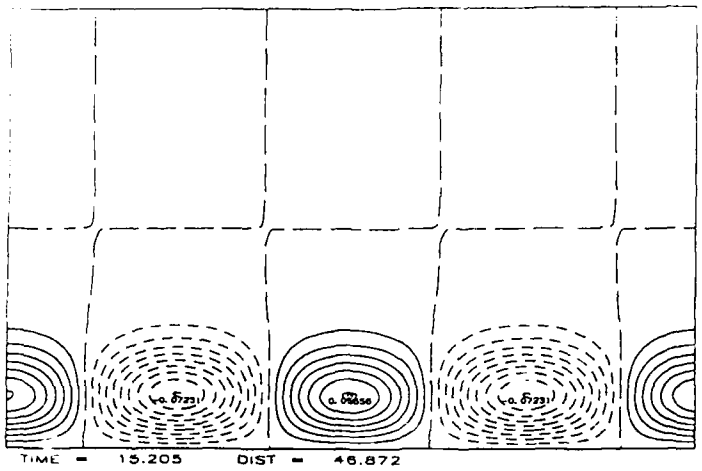

(a) Time = 15.2

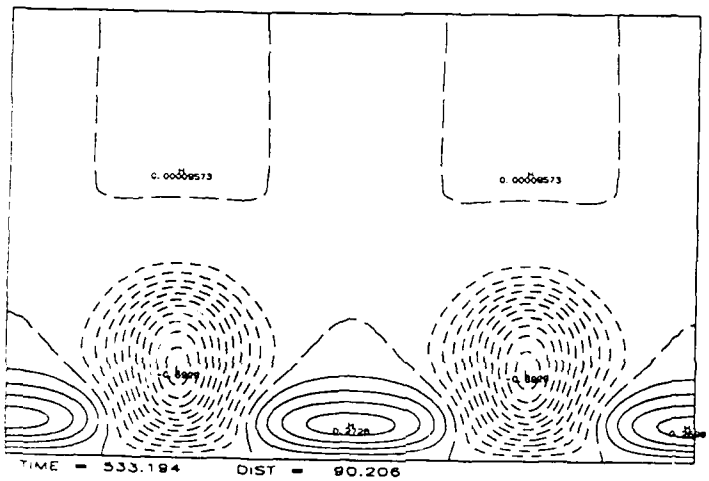

(b) Time = 533

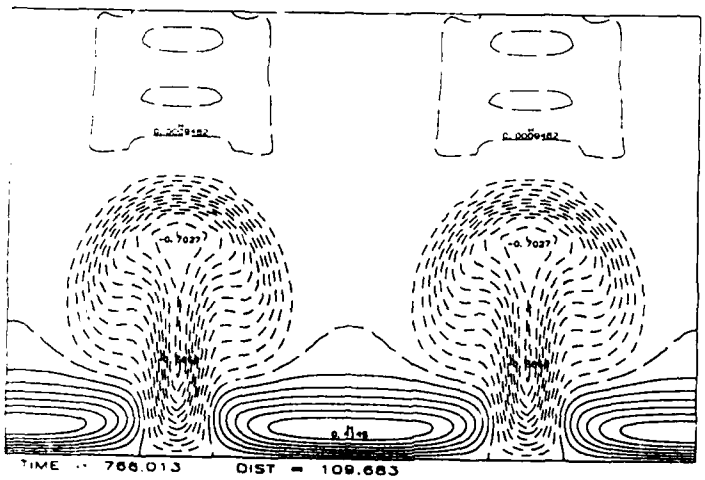

(c) Time = 766

Figure 6. Disturbance u-velocity in y-z plane for Görtler vortex flow at various times.

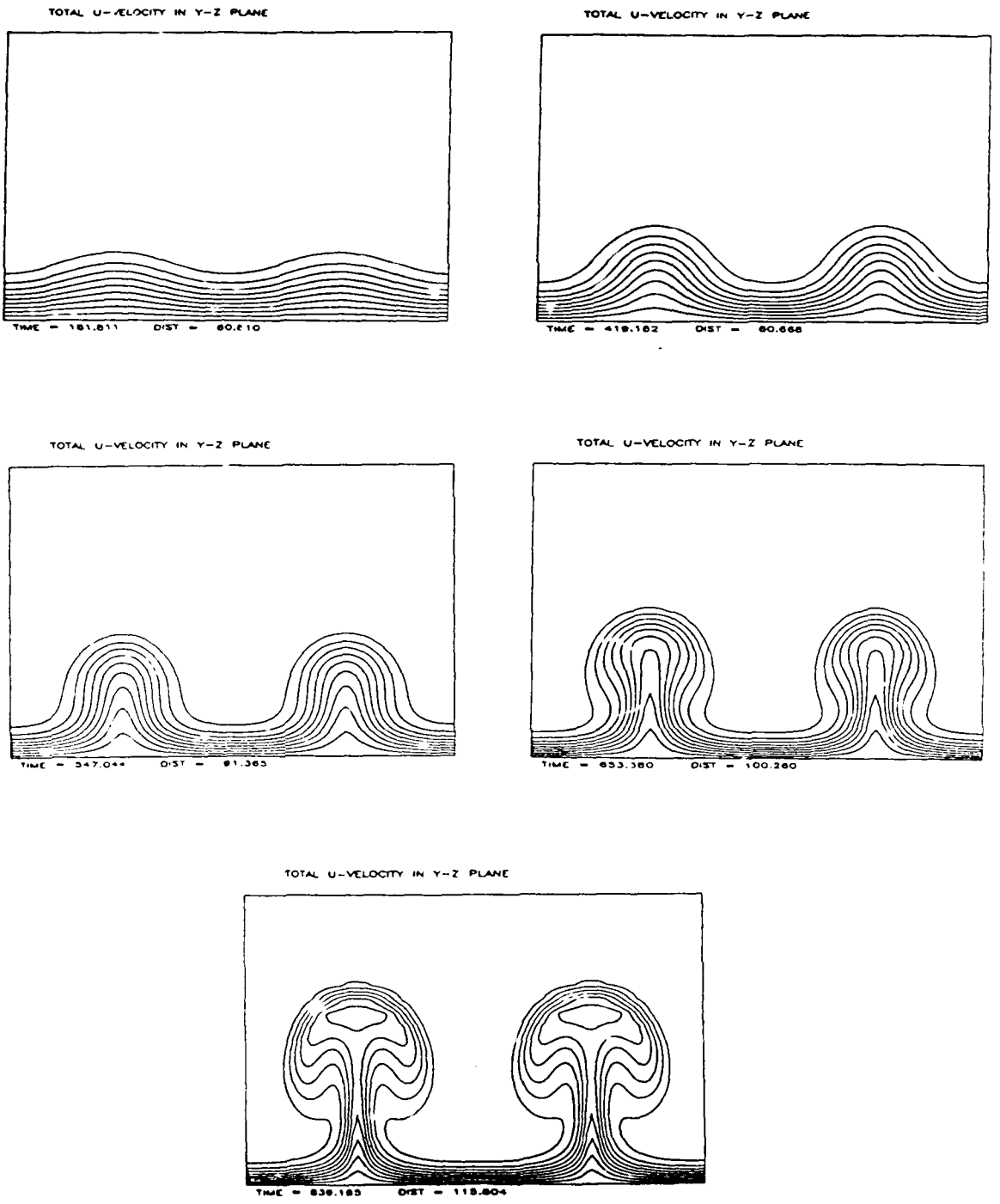

Figure 7(a). Computed iso-contours of the streamwise velocity in the cross stream y-z plane for Görtler vorte . flow. The contours are plotted with velocities 0.1, 0.2,...,0.9.

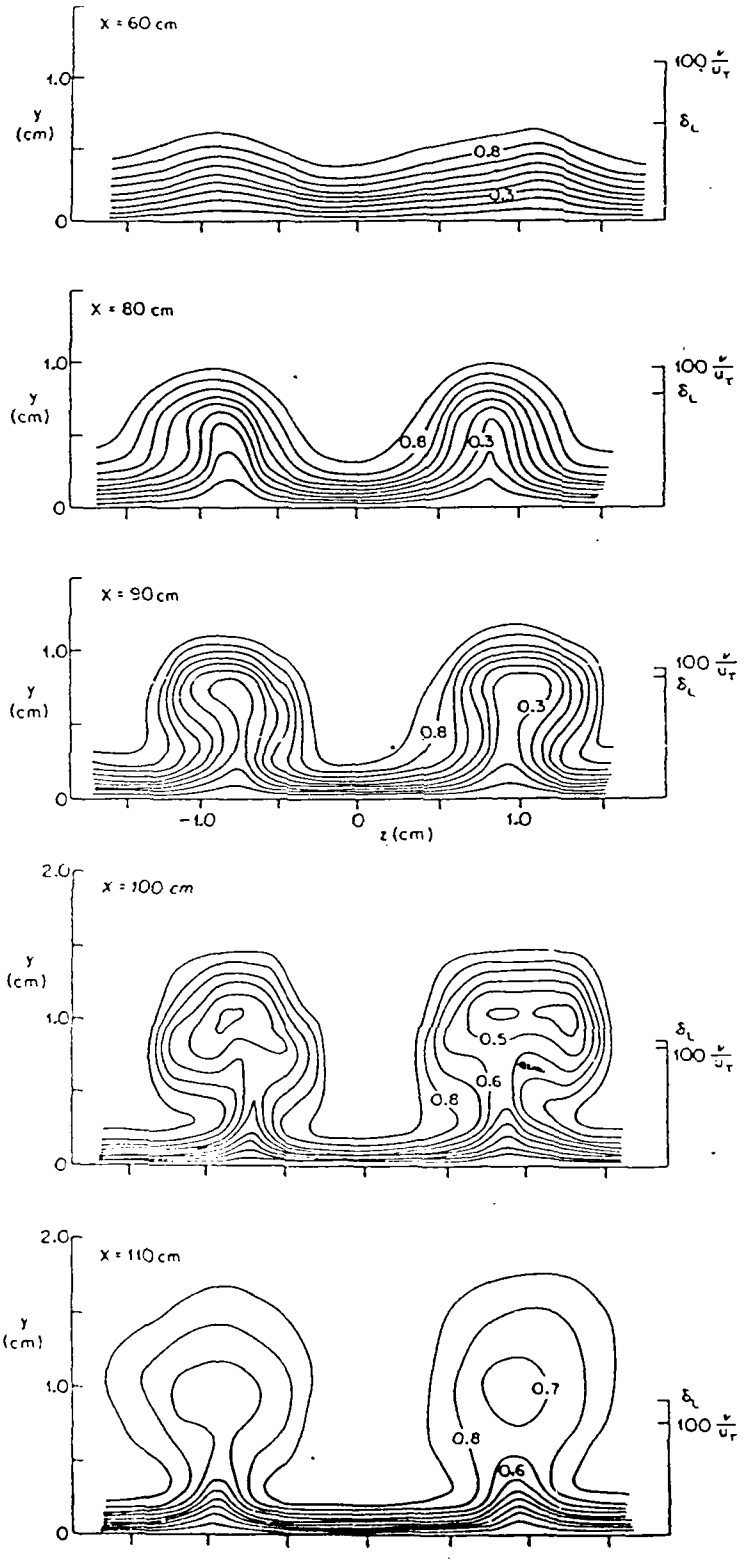

Figure 7(b). Measured (Ref. [14]) iso-contours of the mean streamwise velocity in the cross stream y-z plane. The contours are plotted with velocities 0.1, 0.2,...,0.9.

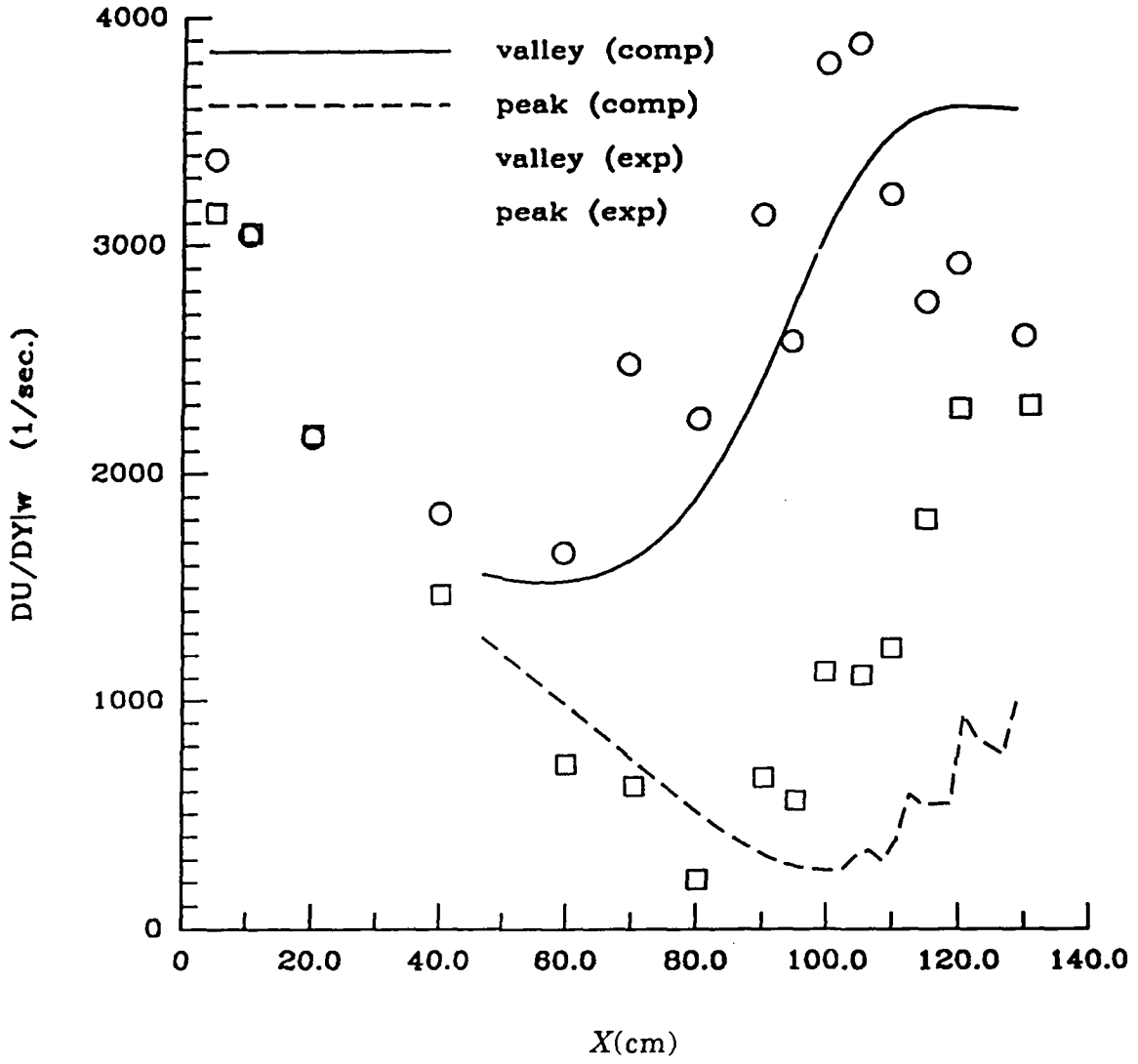

Figure 8(a). A comparison of the computed and experimentally observed (Ref. [14]) development of wall shear *DU/DY* for Görtler vortex flow.

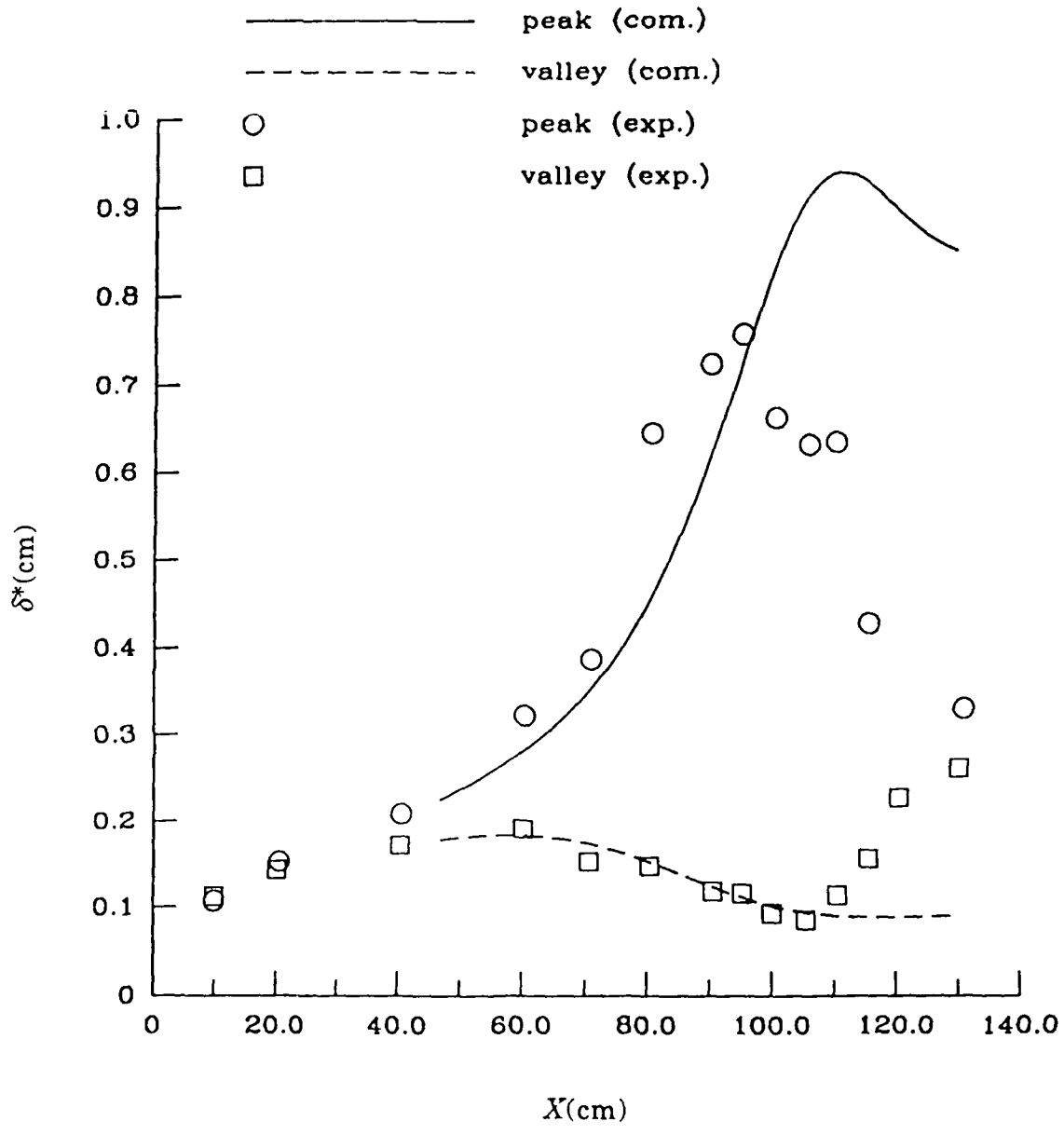

Figure 9(a). A comparison of the computed and experimentally observed (Ref. [19]) displacement thickness vs. streamwise distance.

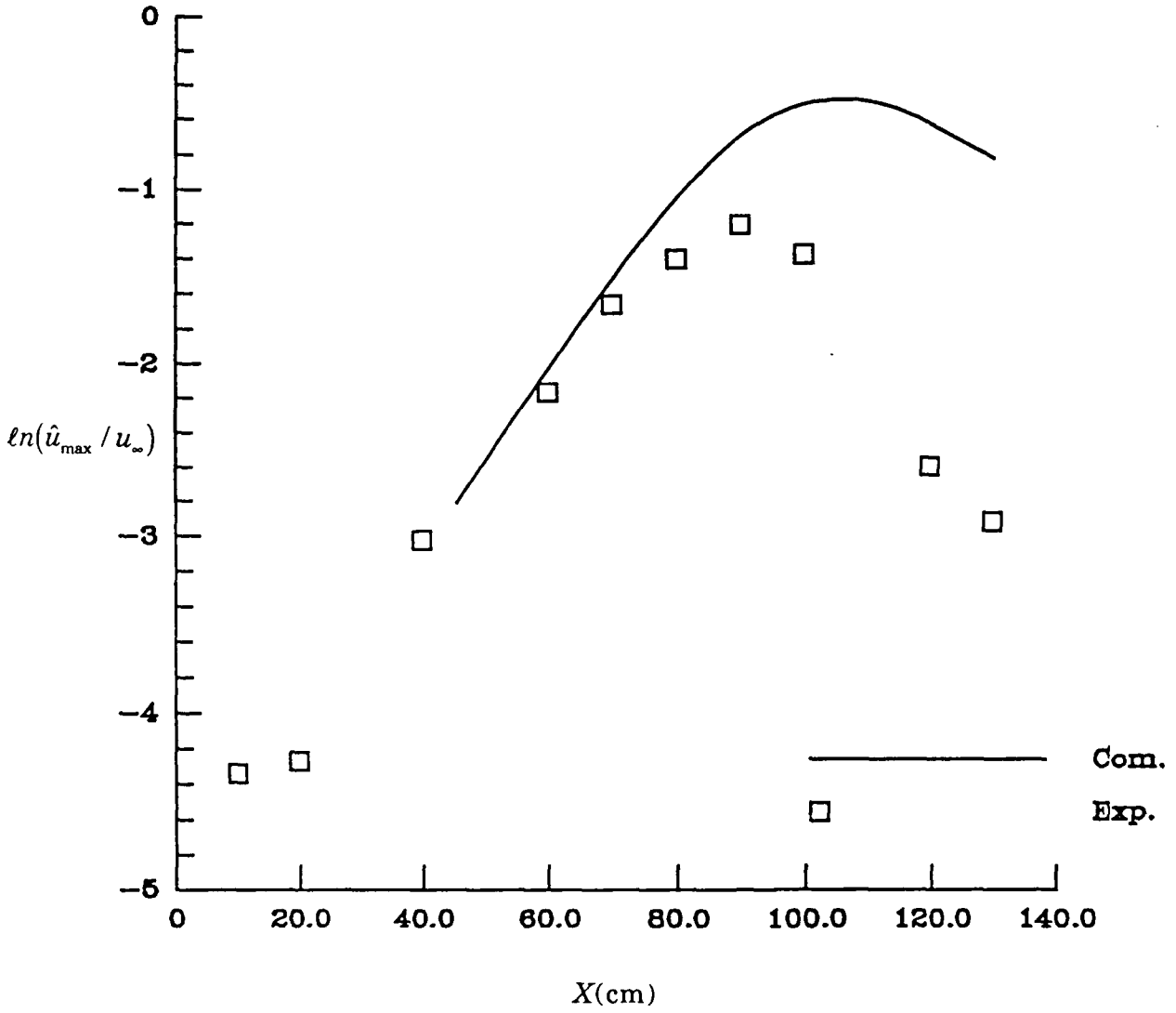

Figure 10(a). The computed and measured (Ref. [14]) rms amplitude of velocity distribution due to the Görtler vortex.

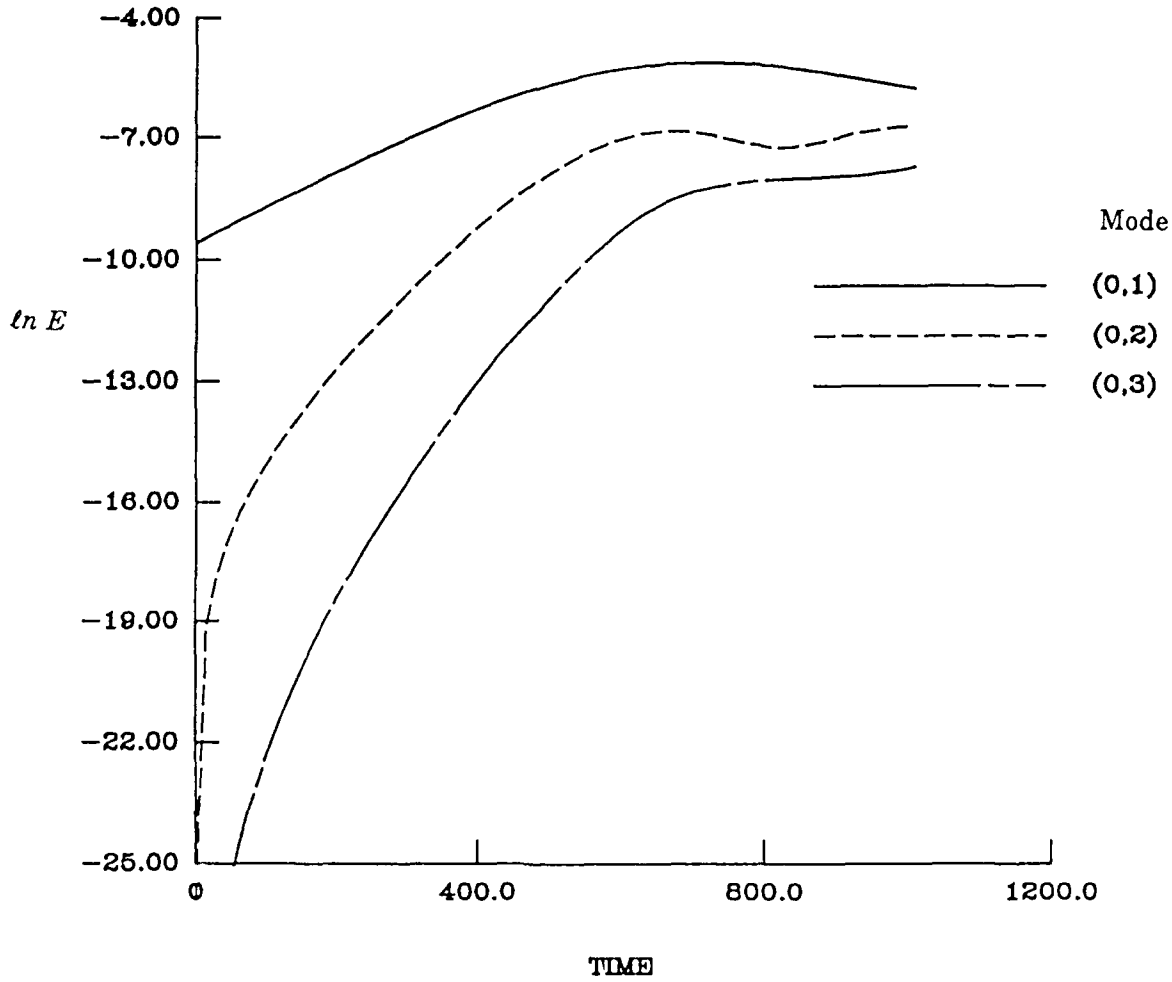

Figure 10(b). Evolution of disturbance energies of various Görtler modes in a boundary layer. The fundamental (0,1) mode continues to have the dominant energy.

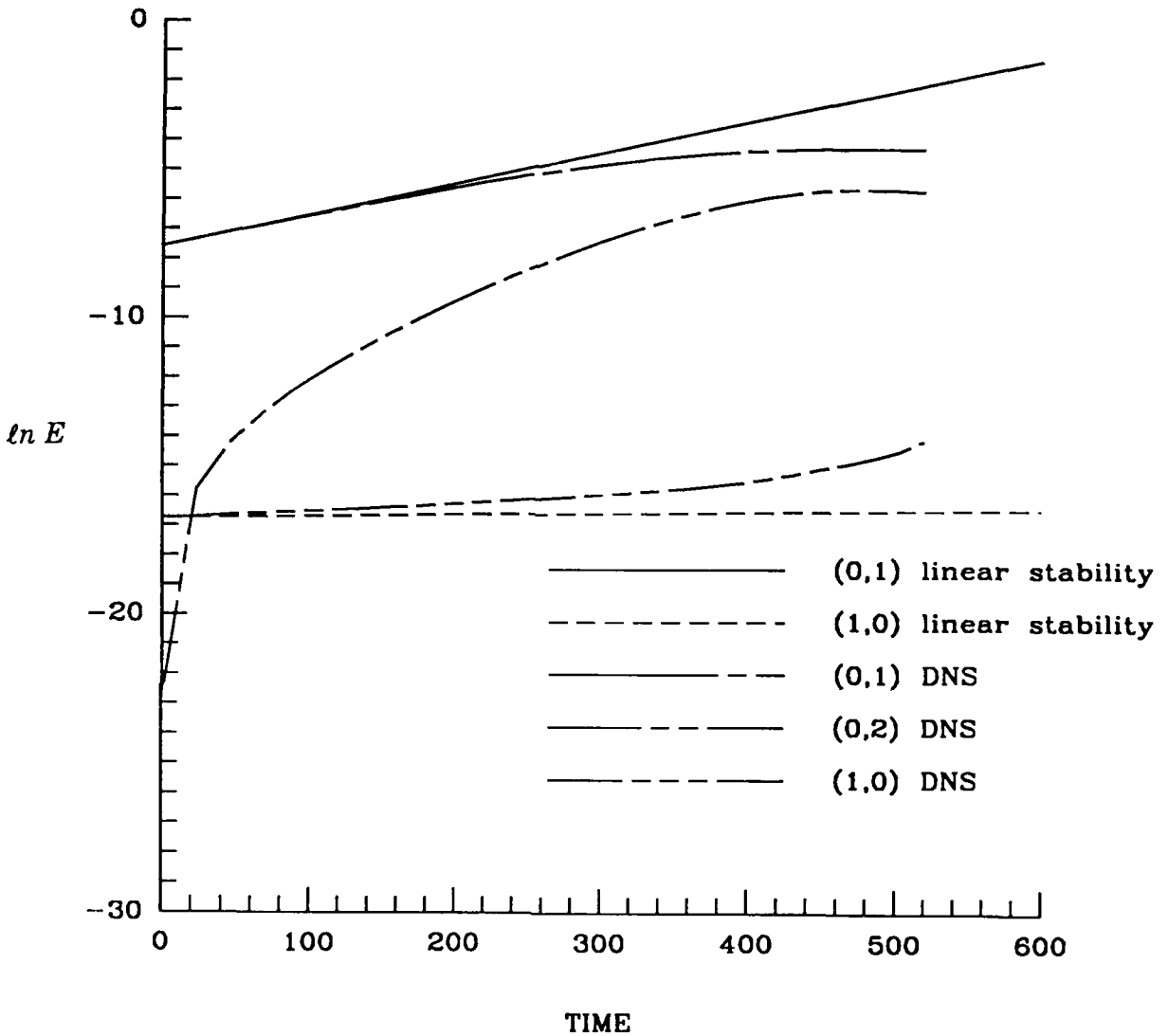

Figure 11. Evolution of energies of various modes using direct numerical simulation and comparison with linear theory results. Due to the presence of Görtler vortex ((0,1)mode), the TS wave ((1,0) mode) grows faster than its linear theory growth rate.

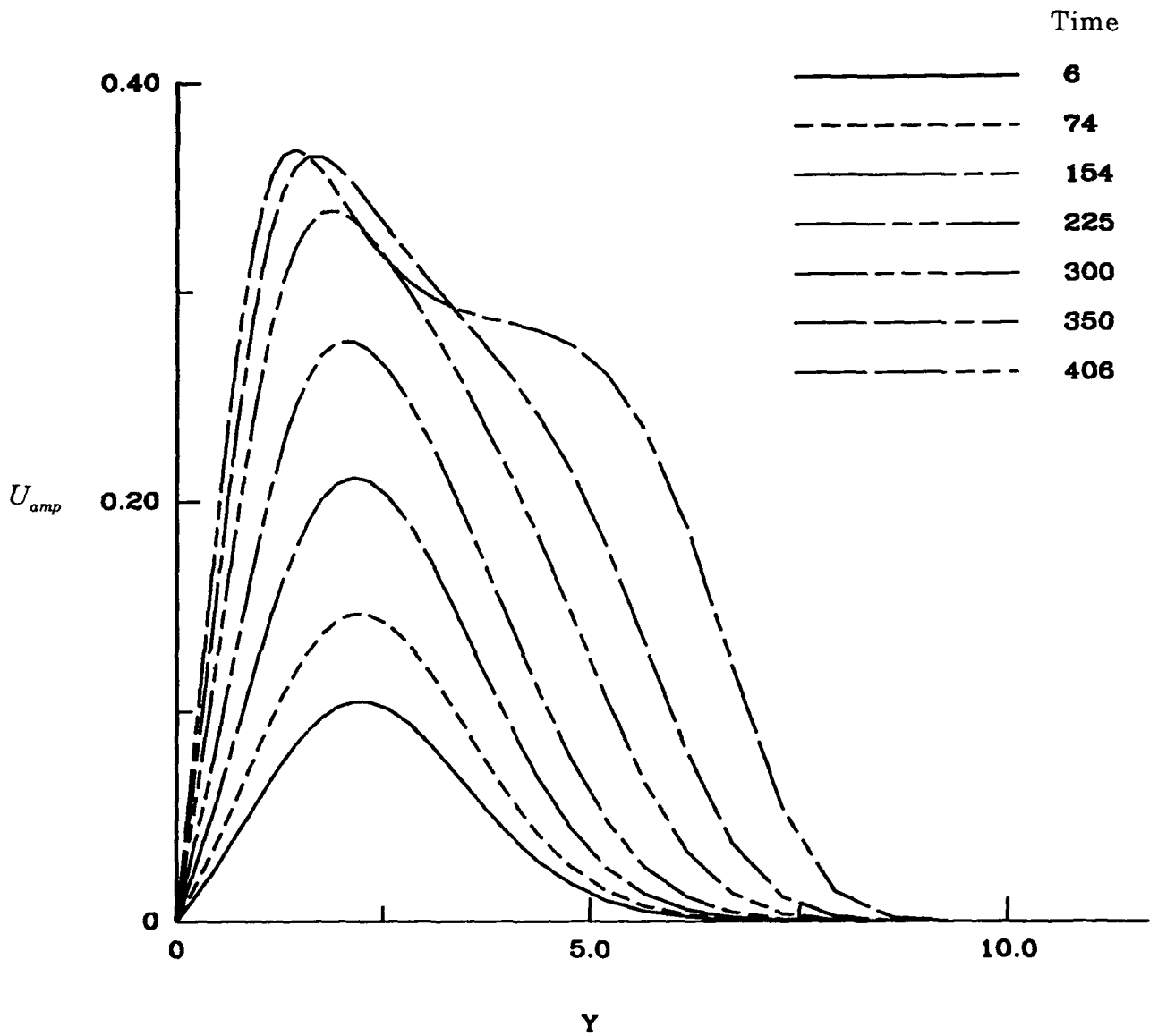

Figure 12(a). Eigenfunctions for the Görtler (0,1) mode at various times.

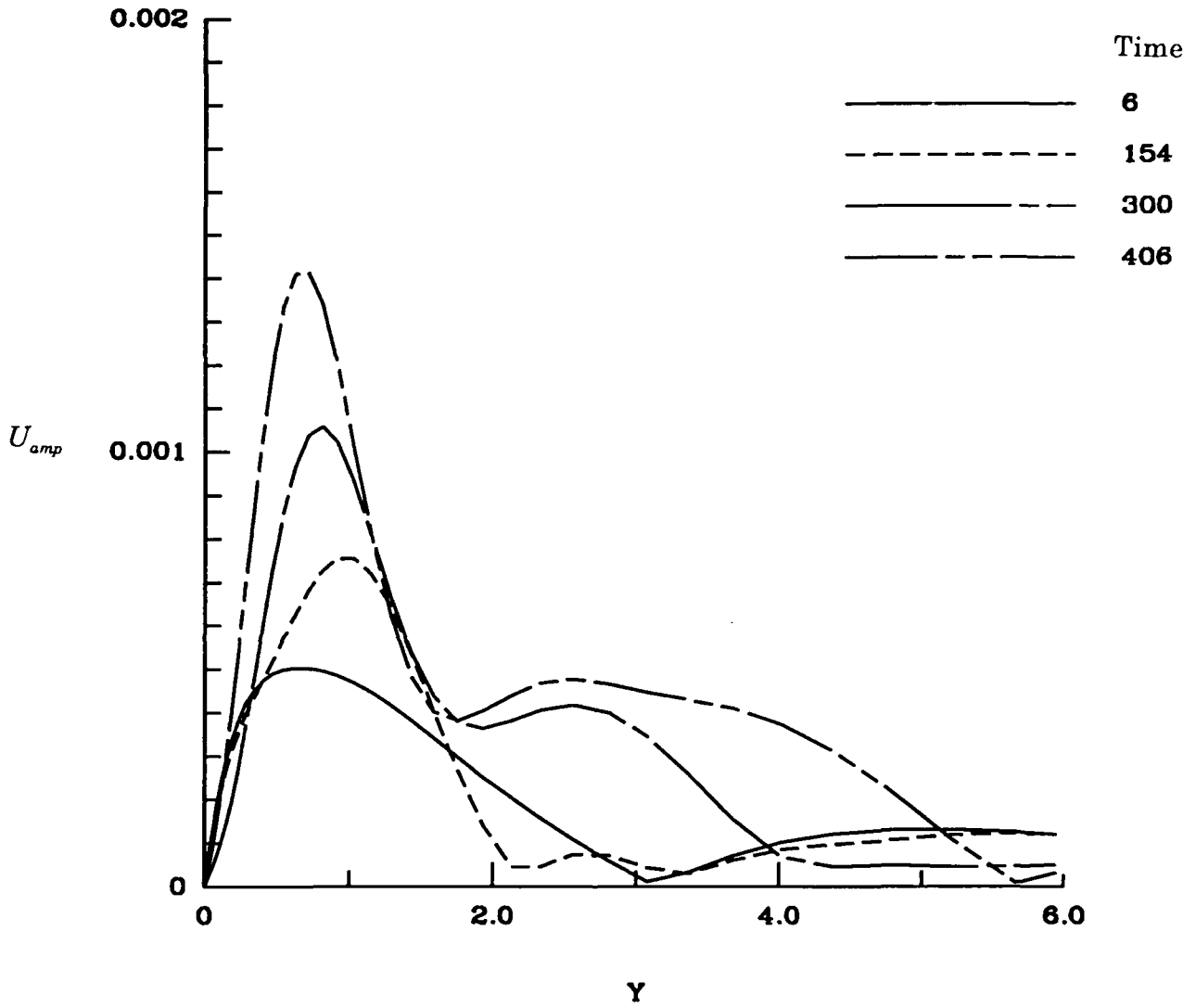

Figure 12(b). Eigenfunctions for the TS (1,0) mode at various times.

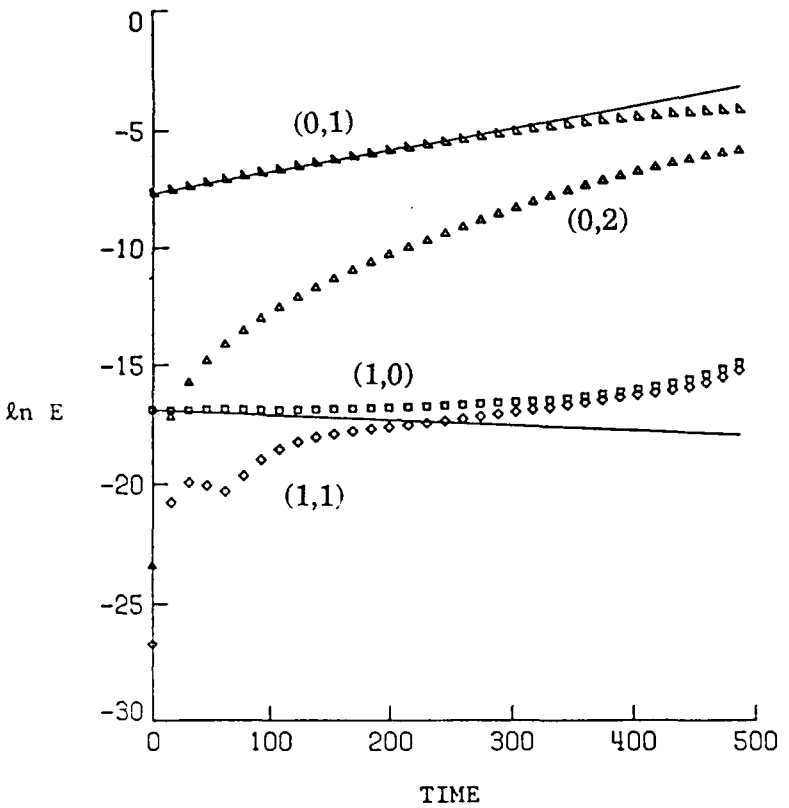

Figure 13. The evolution of the energies of various modes in the presence of a finite-amplitude Görtler vortex ((0,1) mode). The TS wave ((1,0) mode) gets excited.

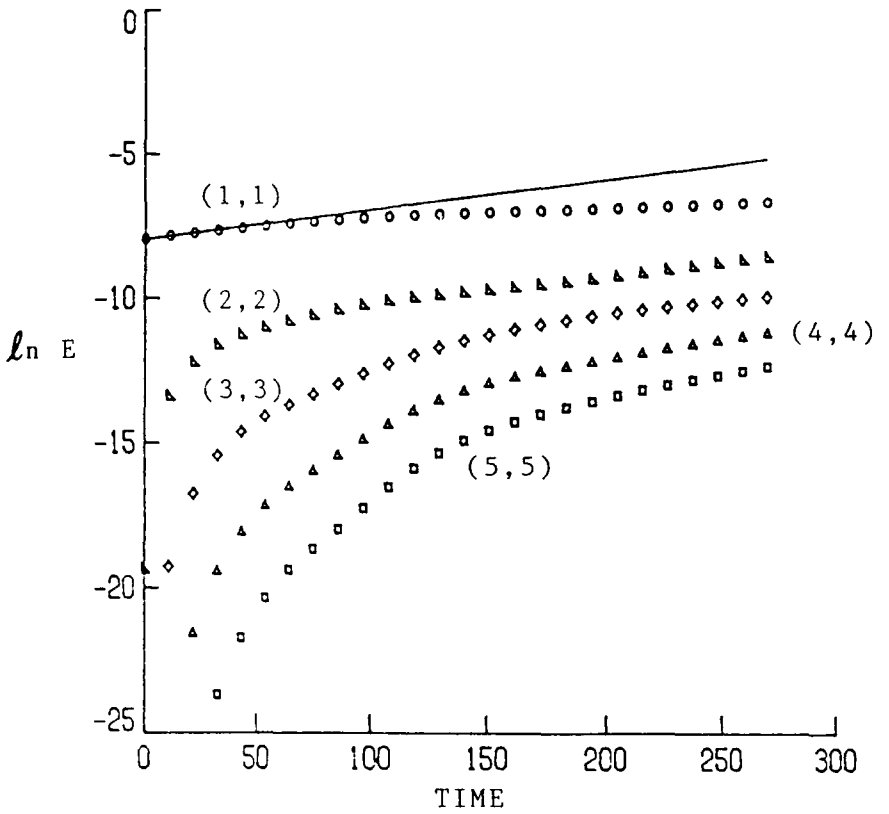

Figure 14. Computed evolution of energies of various modes in the presence of a finite-amplitude crossflow vortex ((1,1) mode) in rotating disk flow. In this calculation $R = 500$, $\alpha = .3751$, $\beta = .0777$. Initial amplitude of the (1,1) mode is 10% of the mean flow.

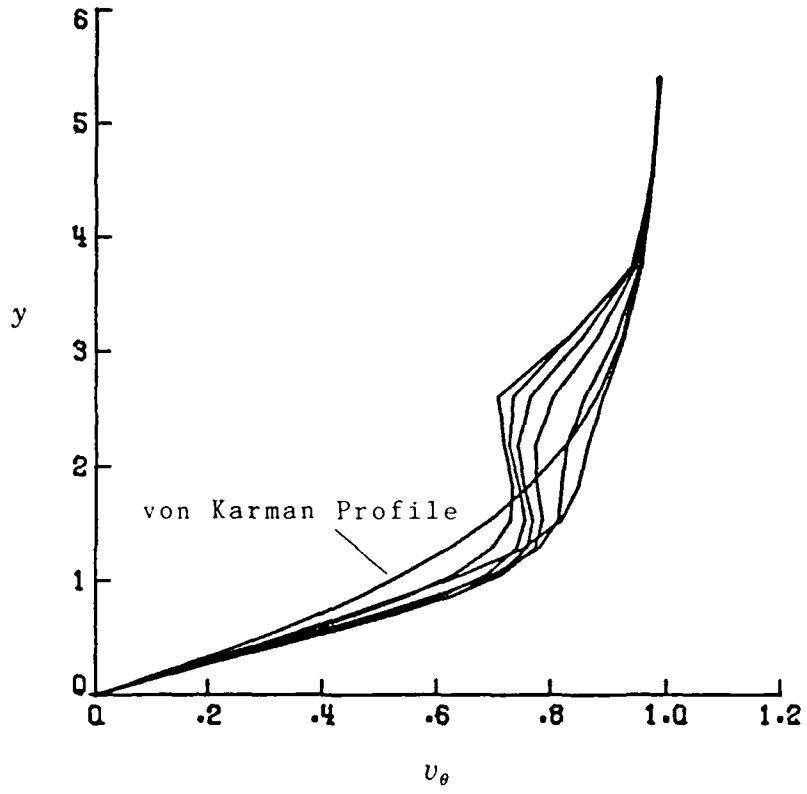

Figure 15. Computed azimuthal velocity profiles in rotating disk flow at a fixed radial location and within 1/2 fundamental wavelength. Time t = 170.

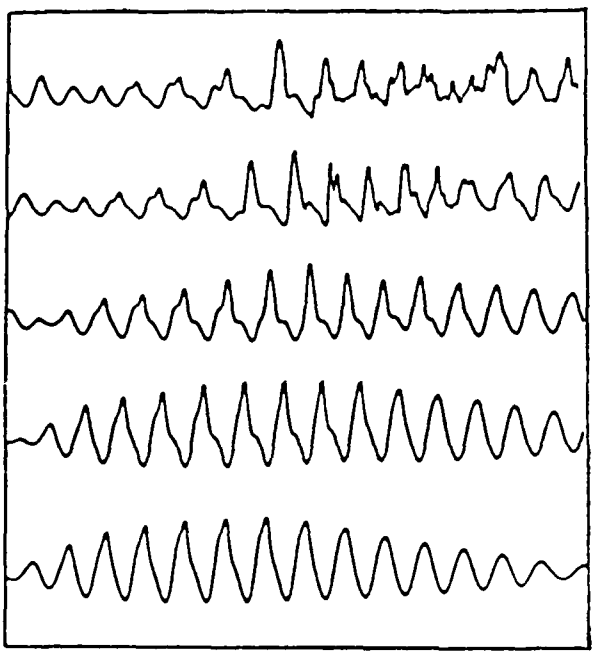

Figure 16(a) Hot-wire traces at various radii near transition in rotating disk boundary layer. Hot-wire is located at $y \cong 1.8$ and it is oriented such that it senses the perturbation in azimuthal velocity component.

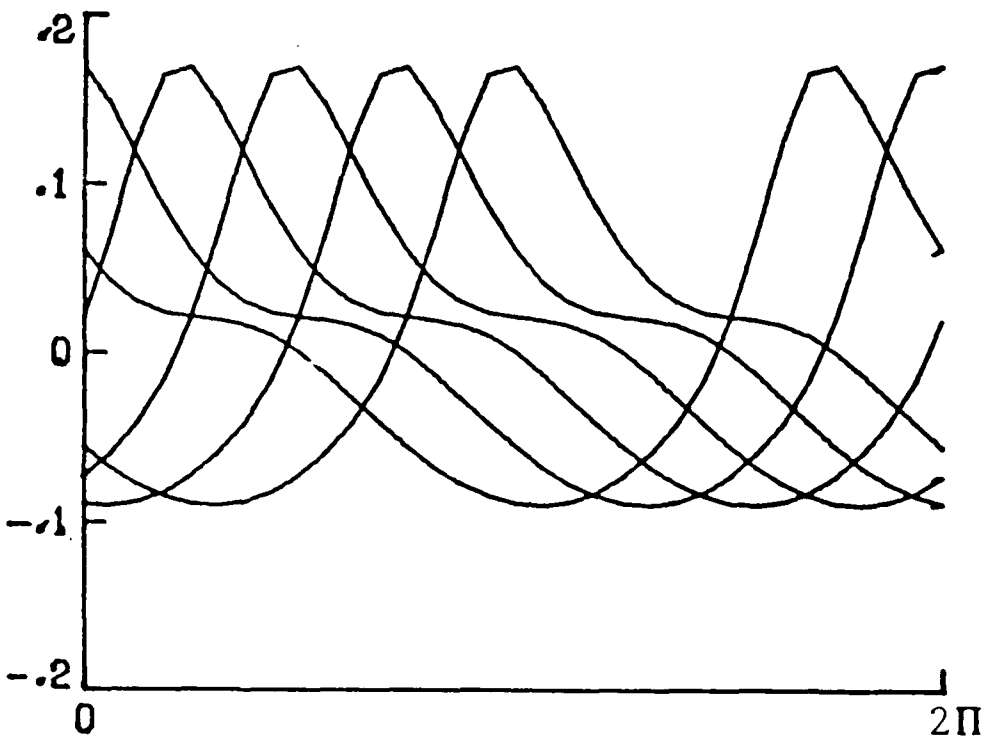

Figure 16(b) Computed traces of azimuthal velocity perturbations at y = 1.8. Only one fundamental wavelength is shown. The calculations are for the conditions of Fig. 14. Time t = 170.

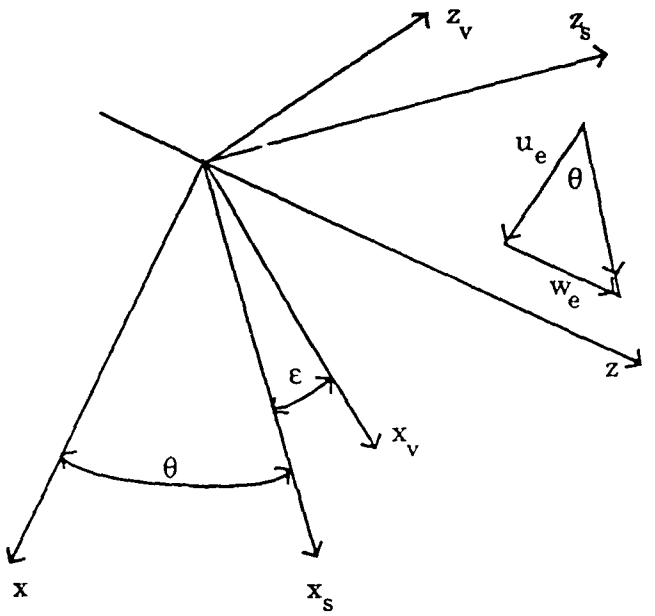

Figure 17. Coordinate system for Falkner-Skan-Cooke boundary layer.

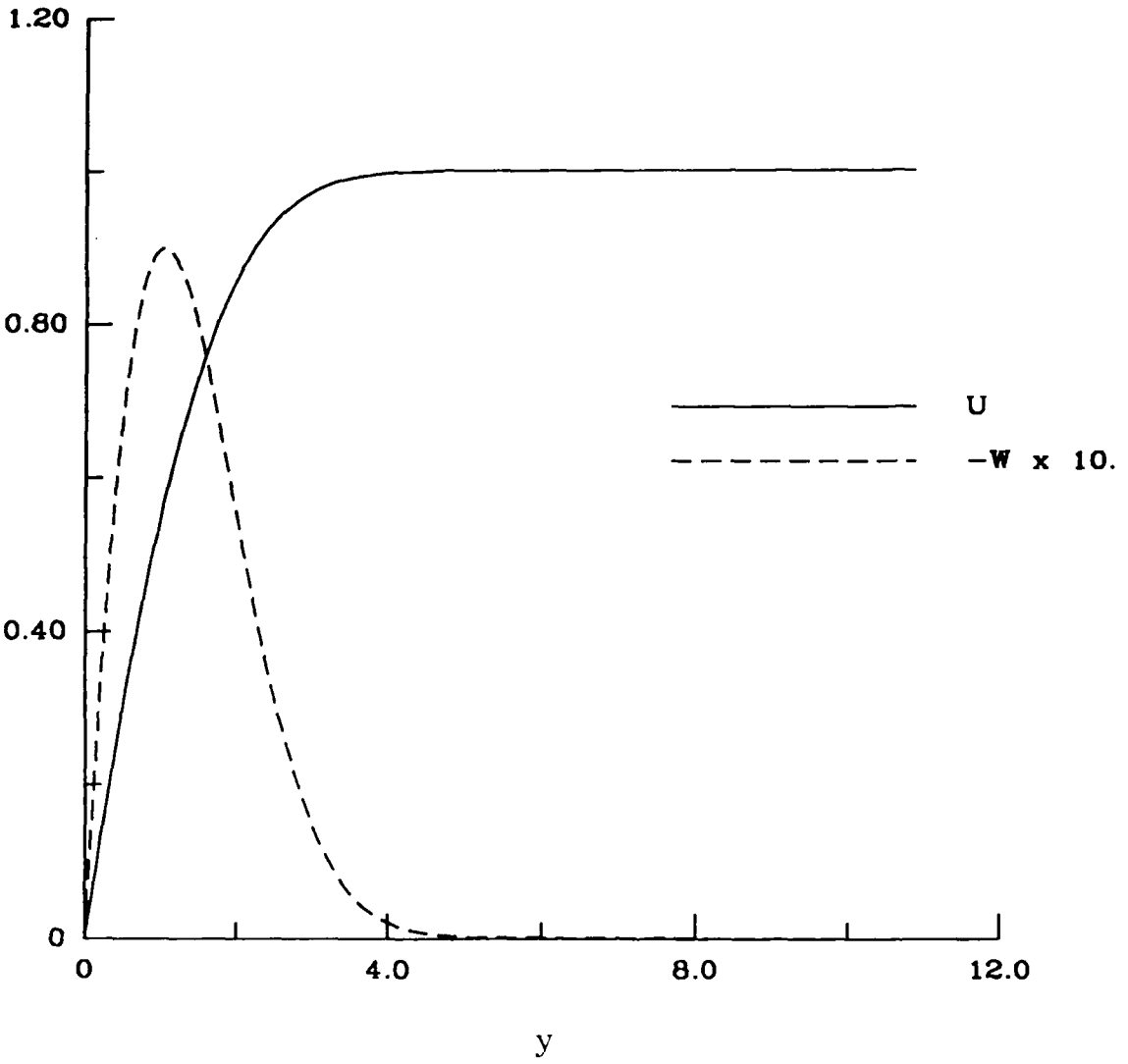

Figure 18. Streamwise and crossflow velocity distribution in Falkner-Skan-Cooke boundary layer.

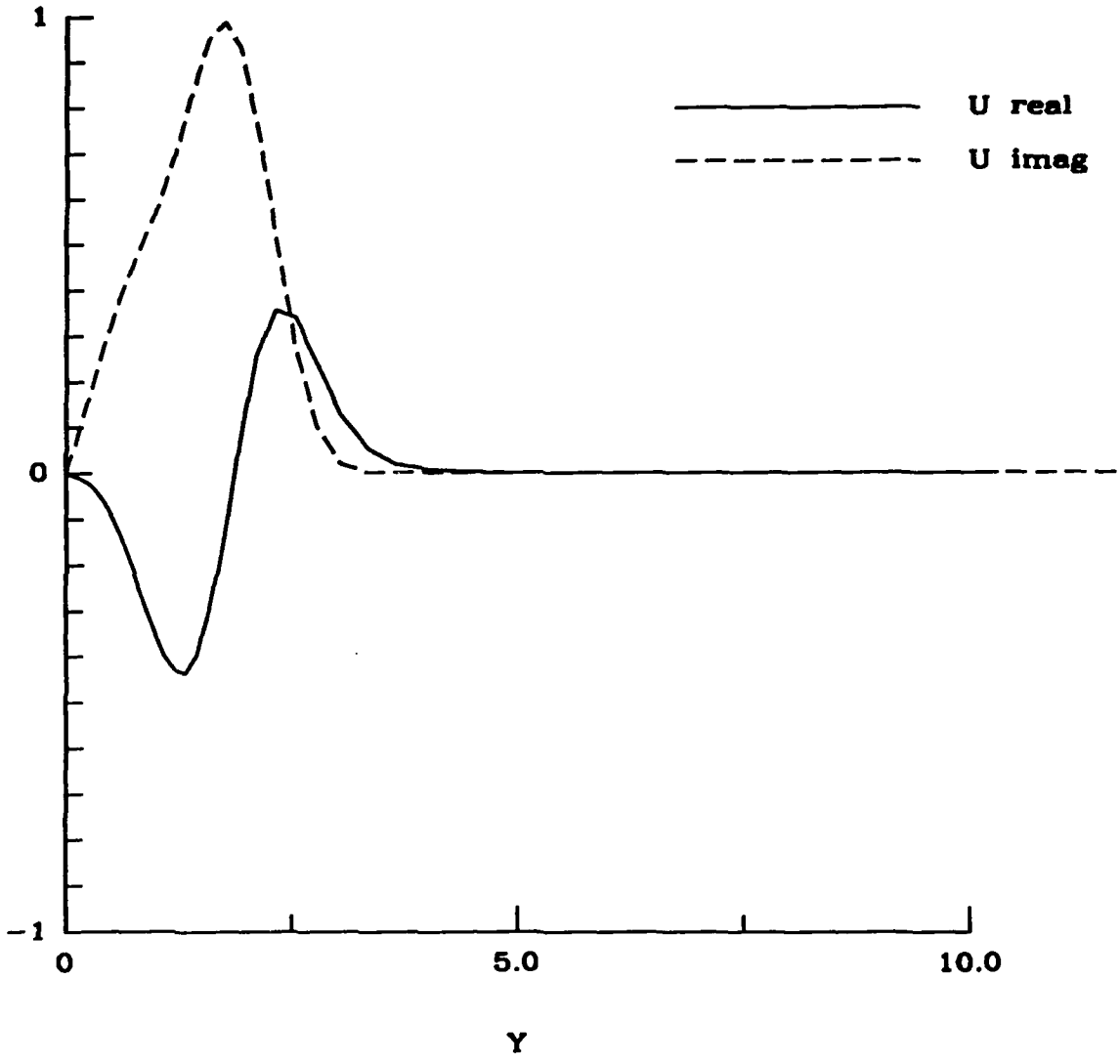

(a) velocity component along the axis of the vortex

Figure 19. Disturbance eigenfunctions for a crossflow vortex in FSC boundary layer.

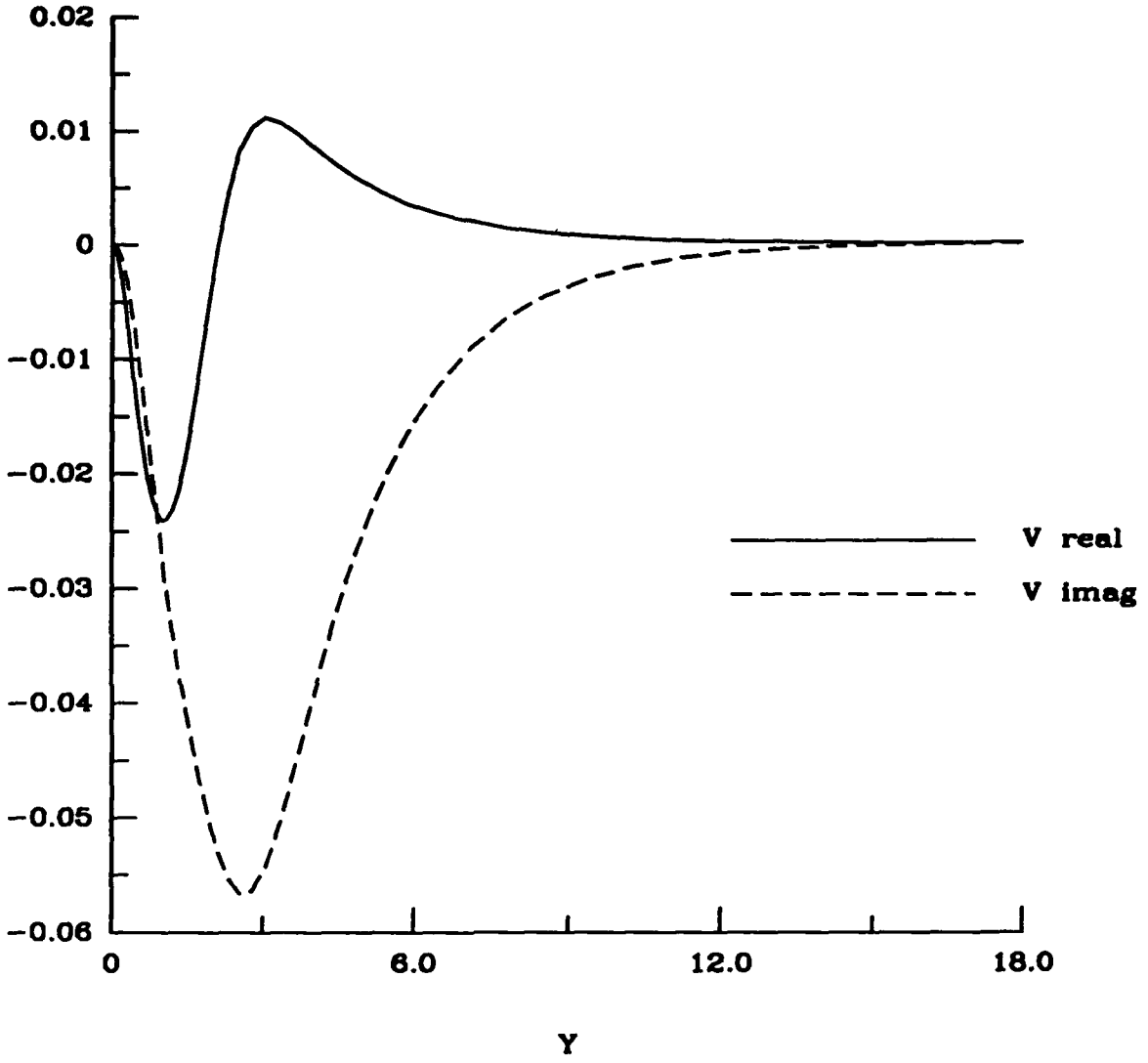

(b) velocity component normal to the surface

Figure 19. Continued.

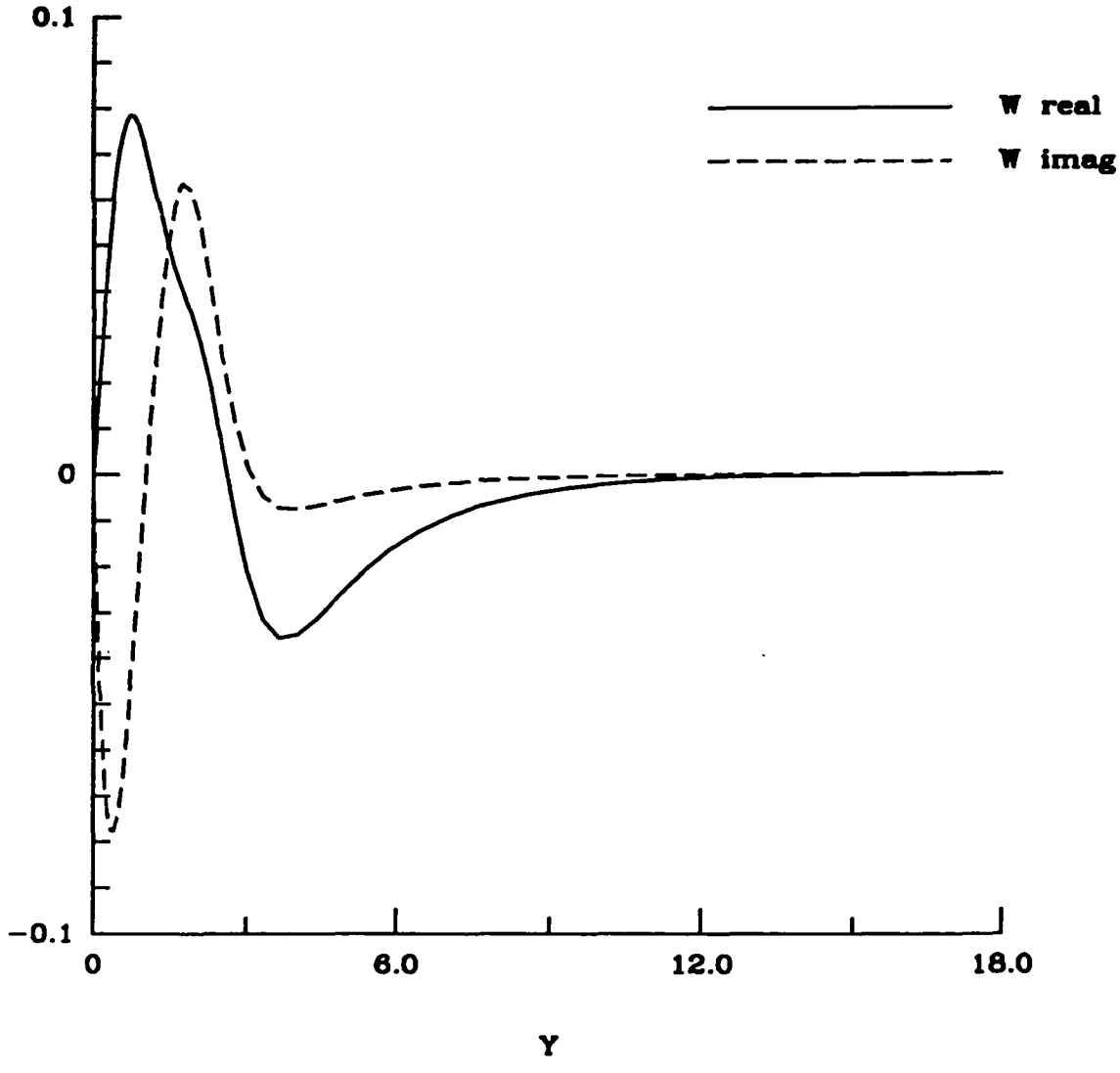

(c) velocity component in the direction of the wavenumber vector

Figure 19. Concluded.

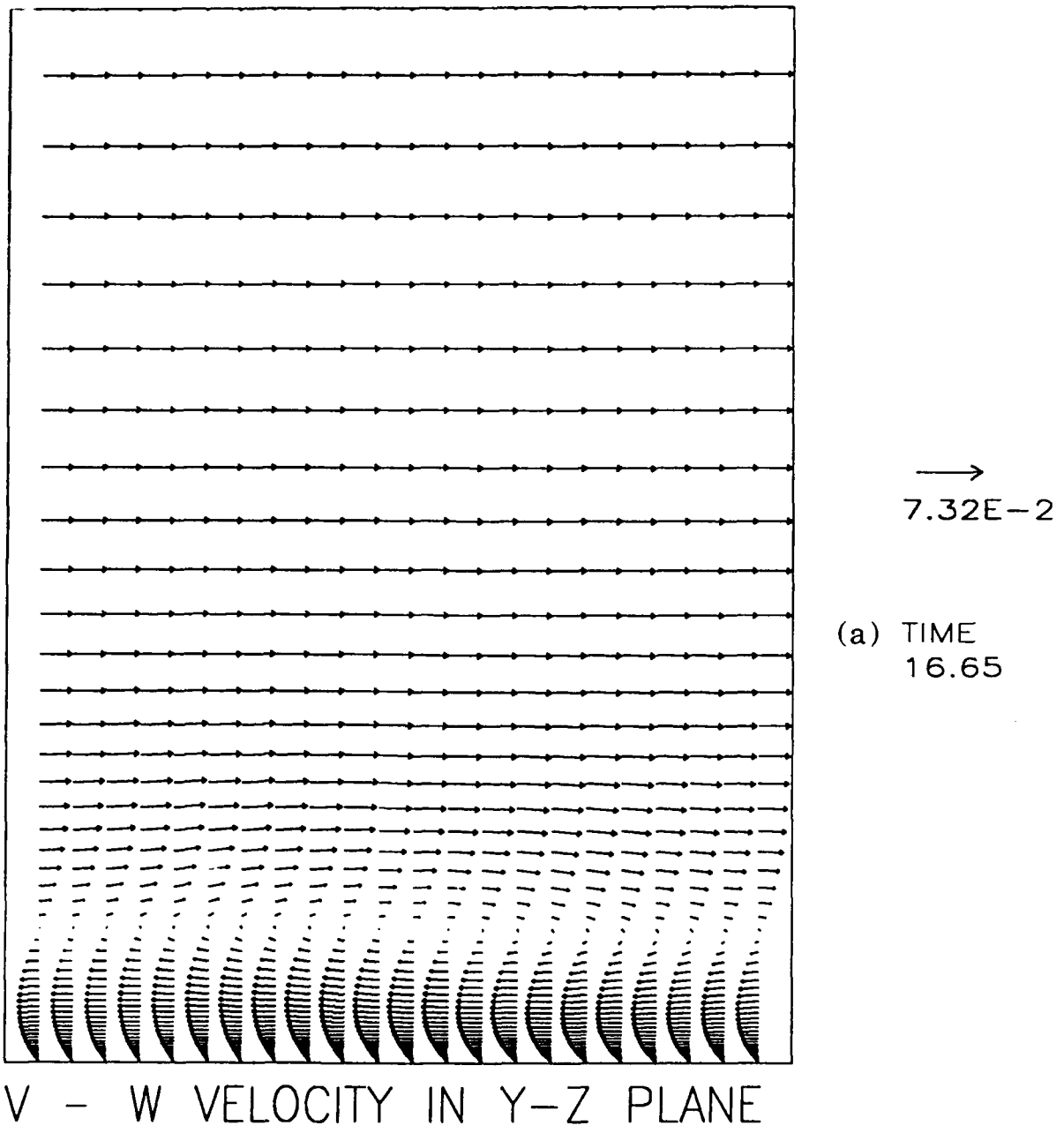

Figure 20. Velocity vector plots in y-z_v plane for a crossflow vortex in FSC boundary layer.

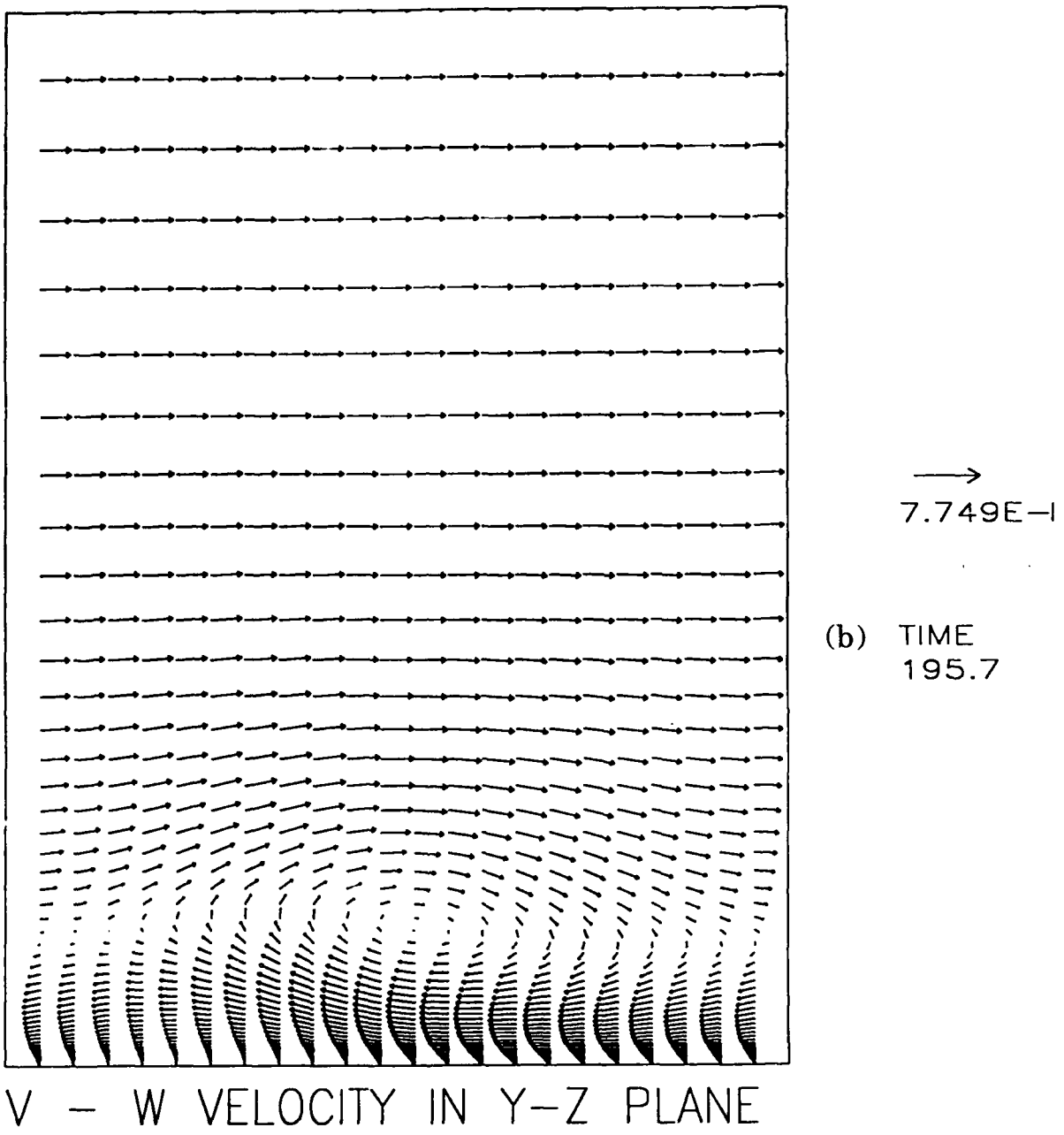

Figure 20. Continued.

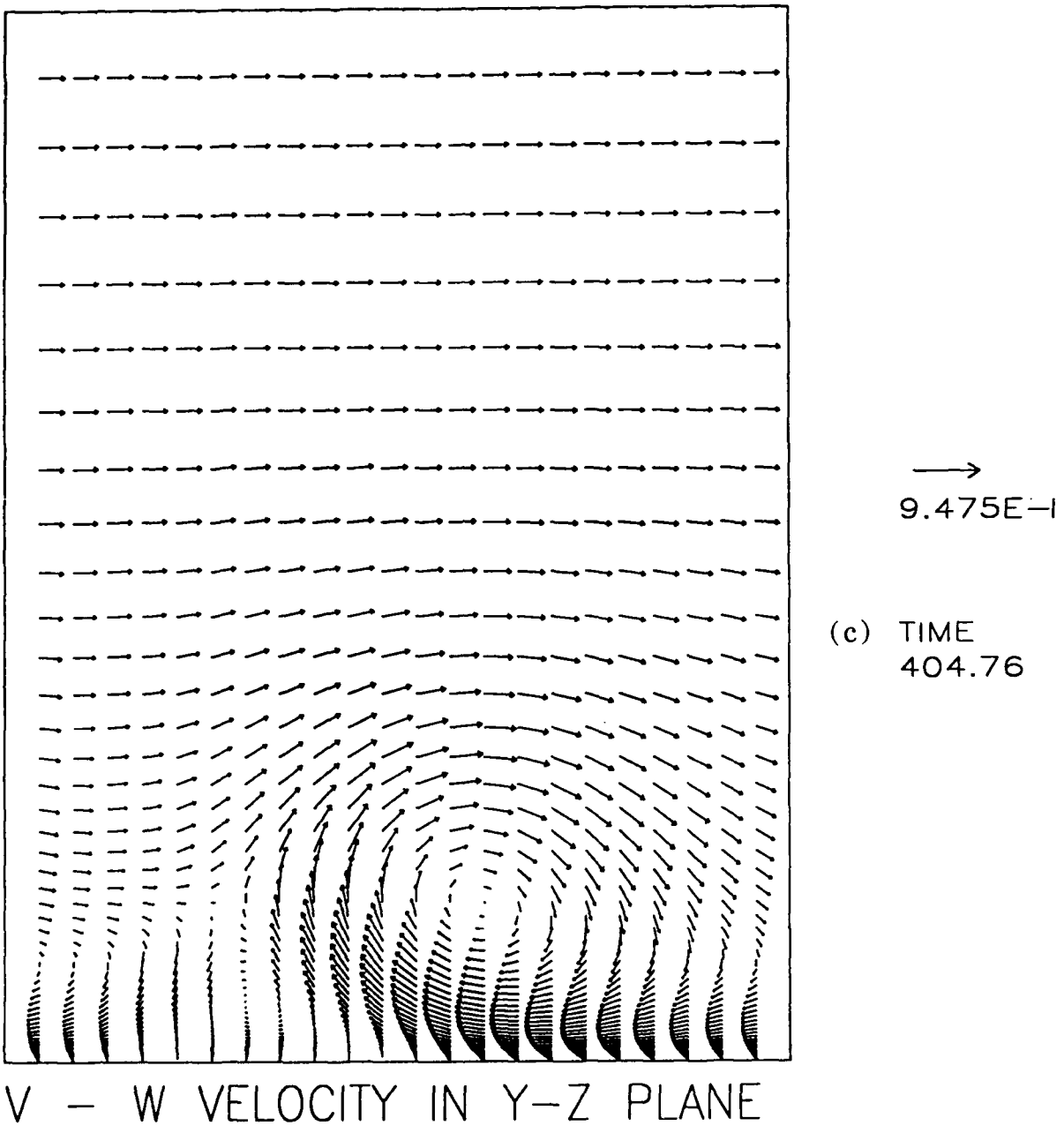

Figure 20. Concluded.

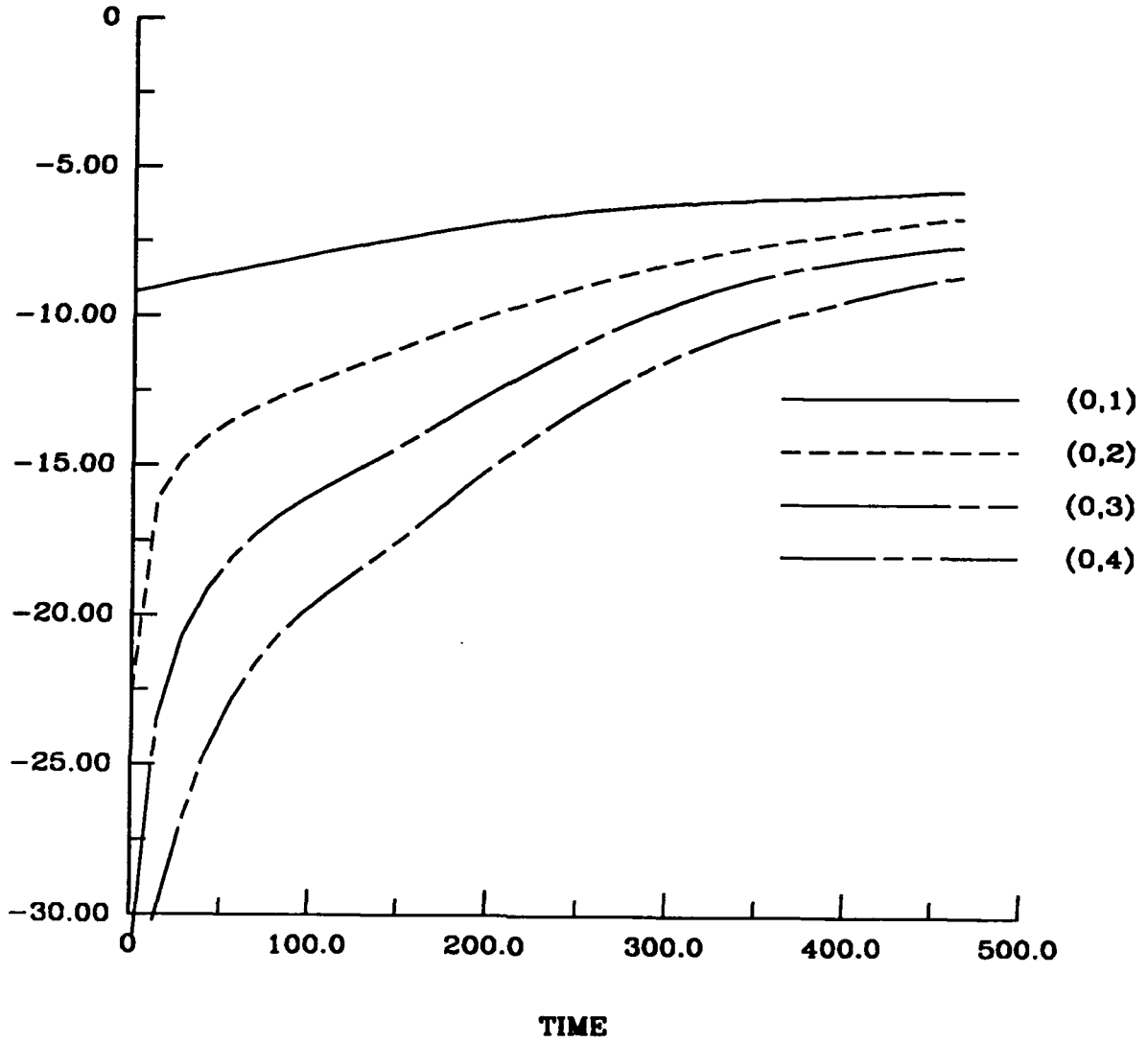

Figure 21. Evolution of energies of various modes in the FSC boundary layer at R = 800. The initial amplitude of the fundamental stationary crossflow vortex ((0,1) mode) is 5 percent.

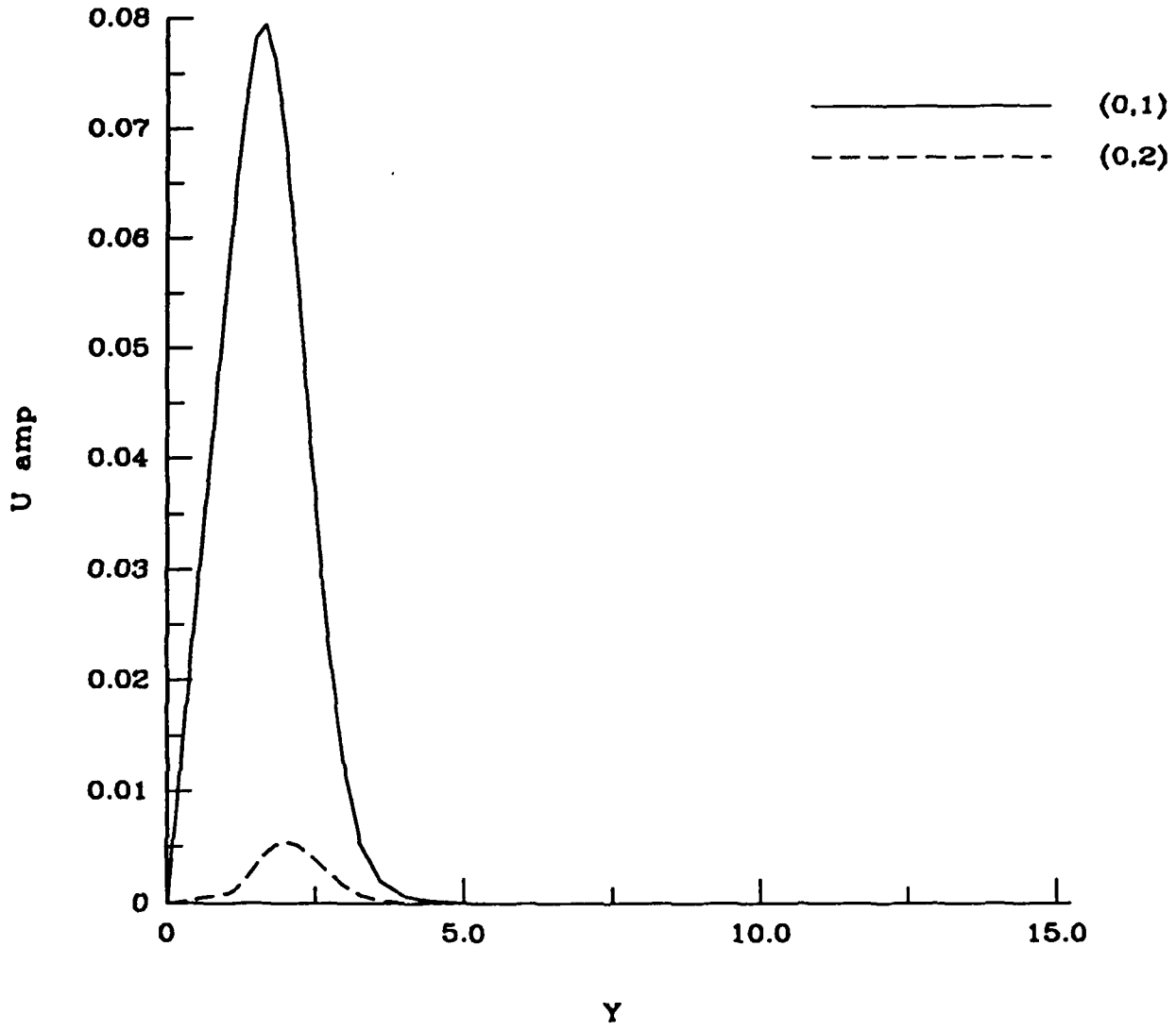

(a) Time = 34

Figure 22. Disturbance u profiles for the fundamental and superharmonic at various times in the presence of a finite amplitude crossflow vortex.

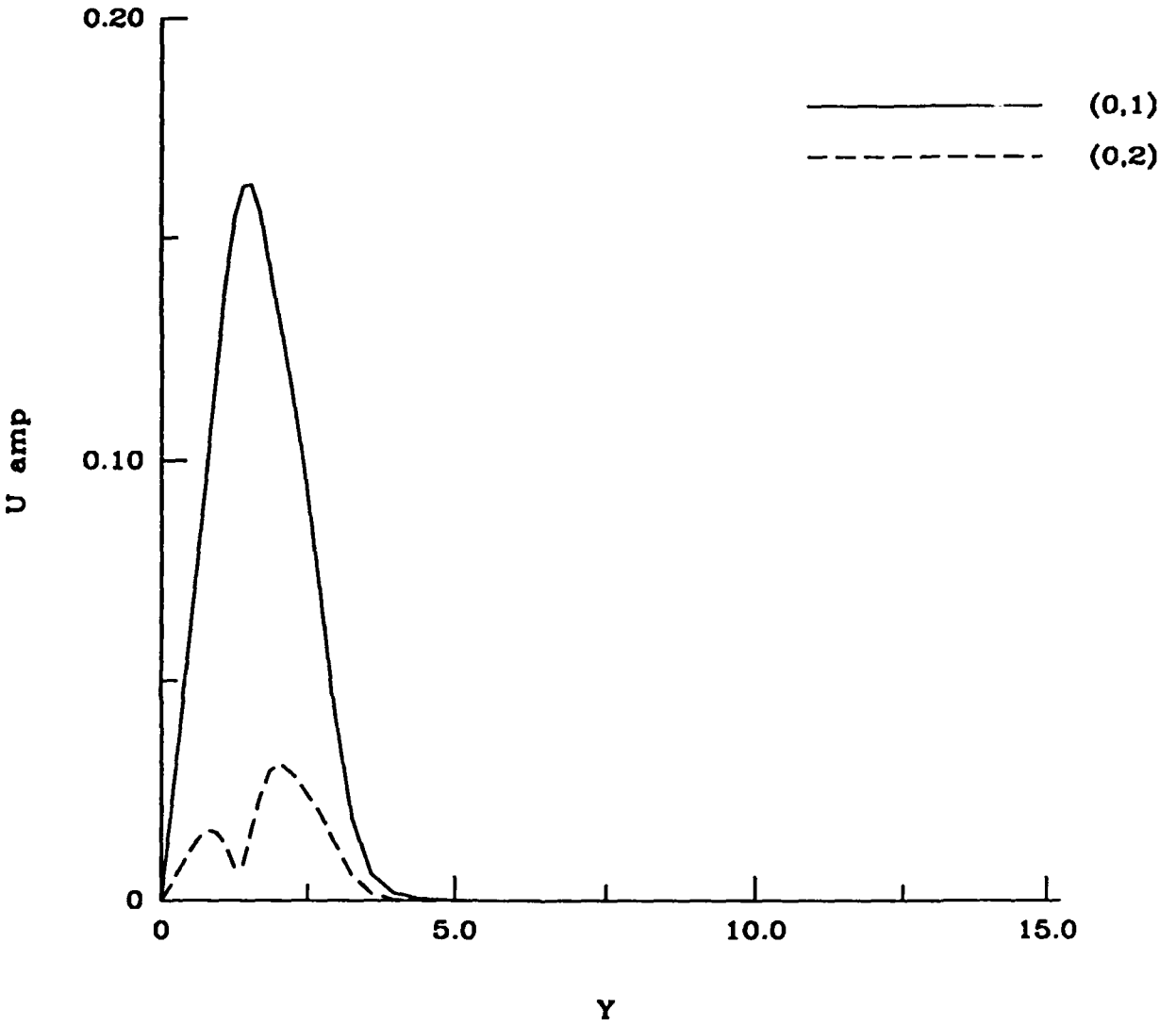

(b) Time = 165

Figure 22. Continued.

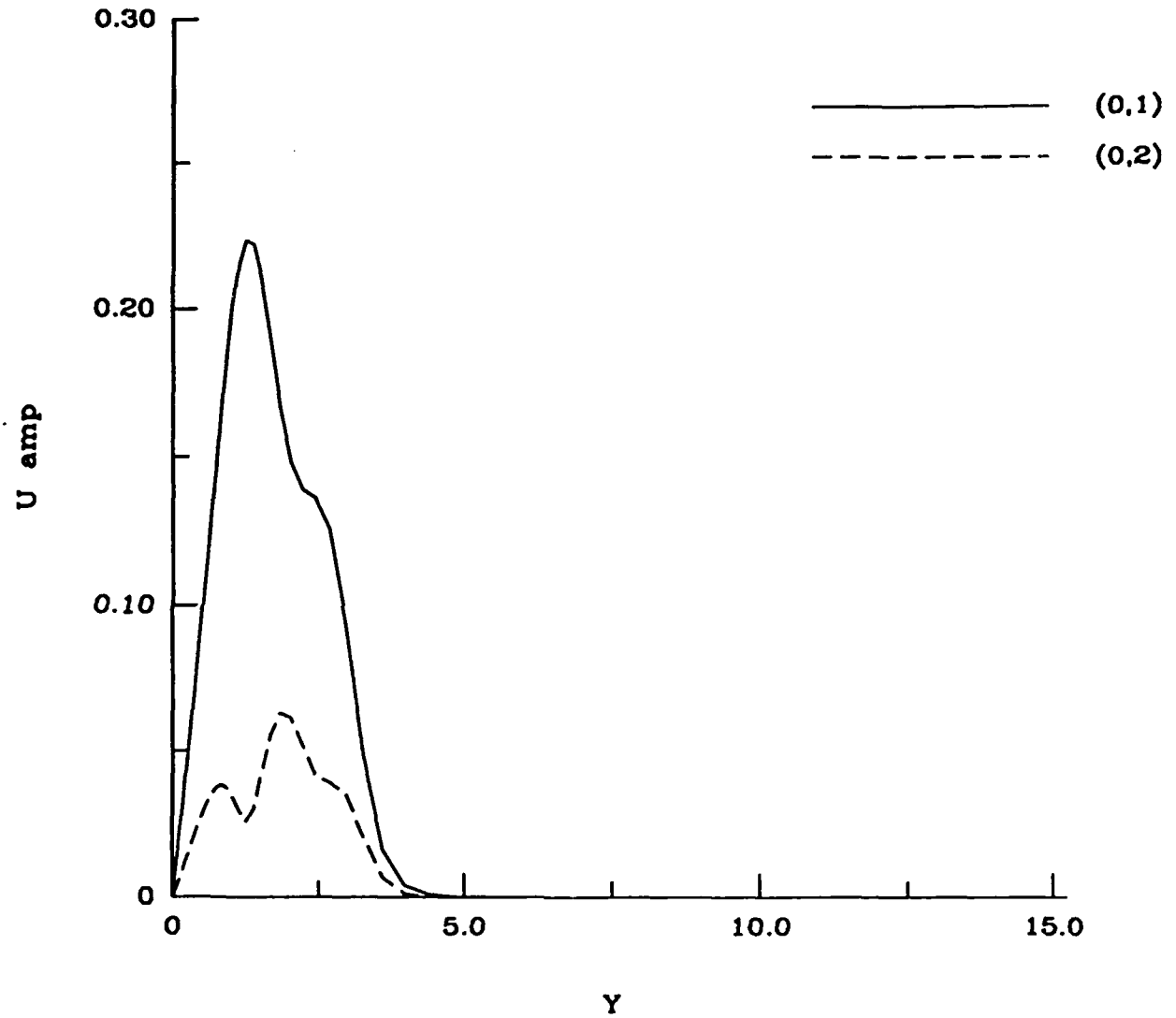

(c) Time = 239

Figure 22. Continued.

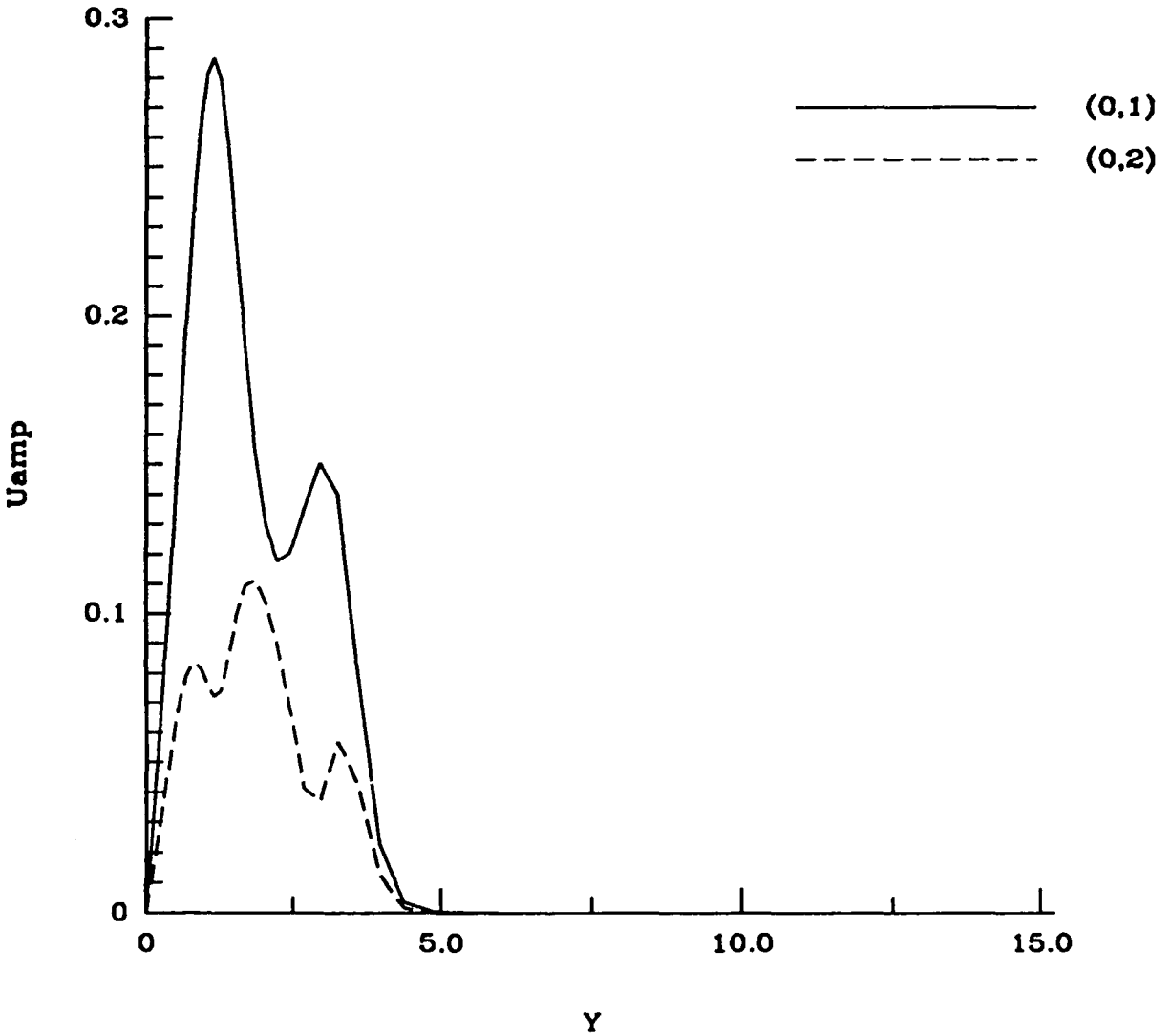

(d) Time = 327

Figure 22. Concluded.

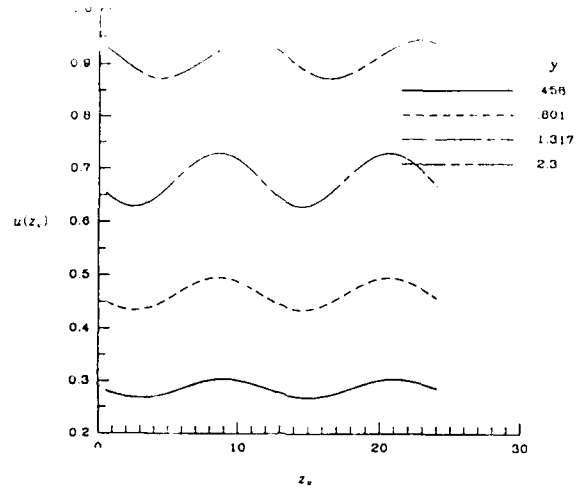

(a) Time = 16

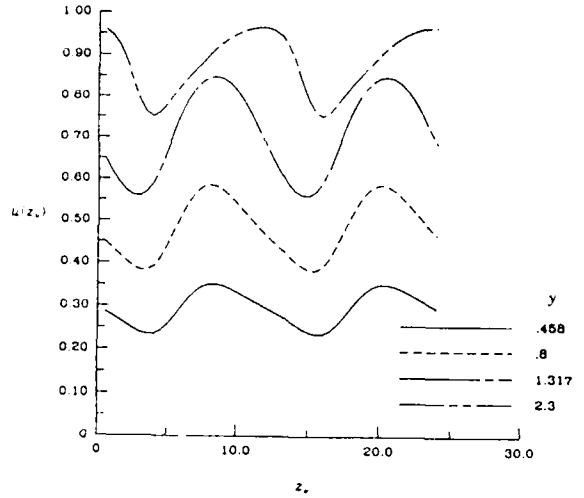

(b) Time = 195

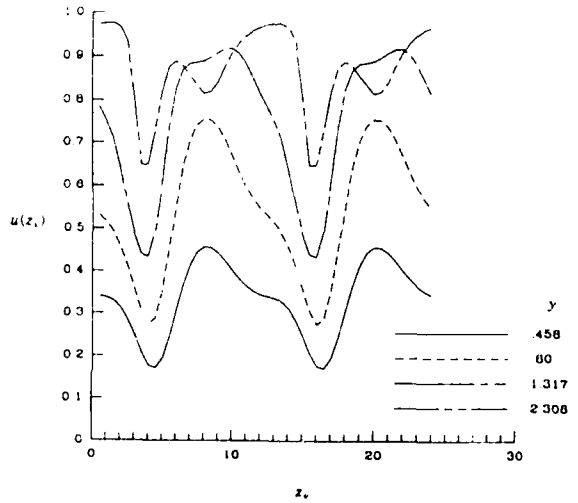

(c) Time = 355

Figure 23. Computational trace of the velocity component along the axis of the crossflow vortex at three different times and at various heights from the surface for FSC boundary layer. Two wave period are shown.

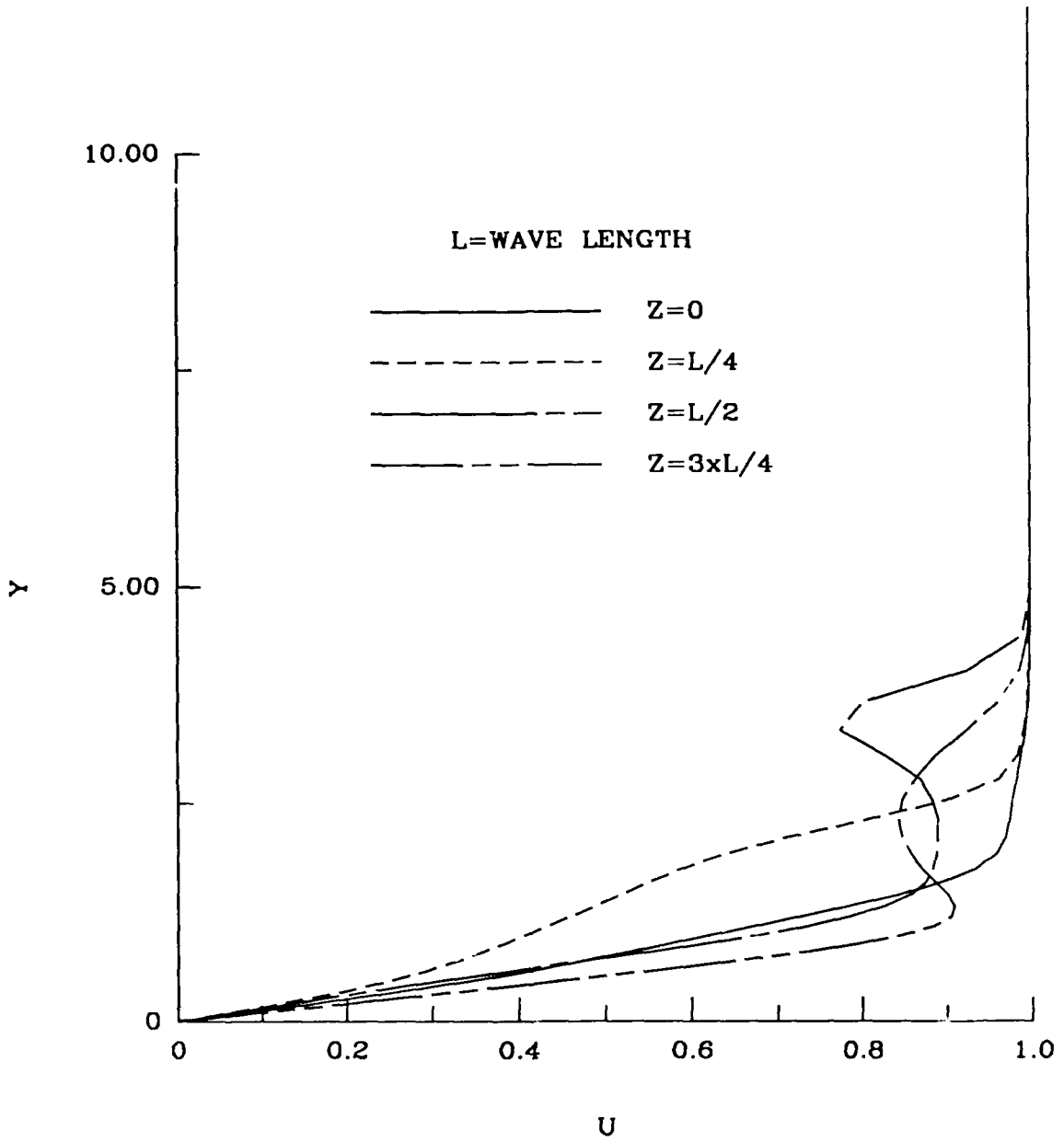

(a) velocity component in the direction of the vortex axis

Figure 24. Velocity components at Time = 355 and various spanwise location.

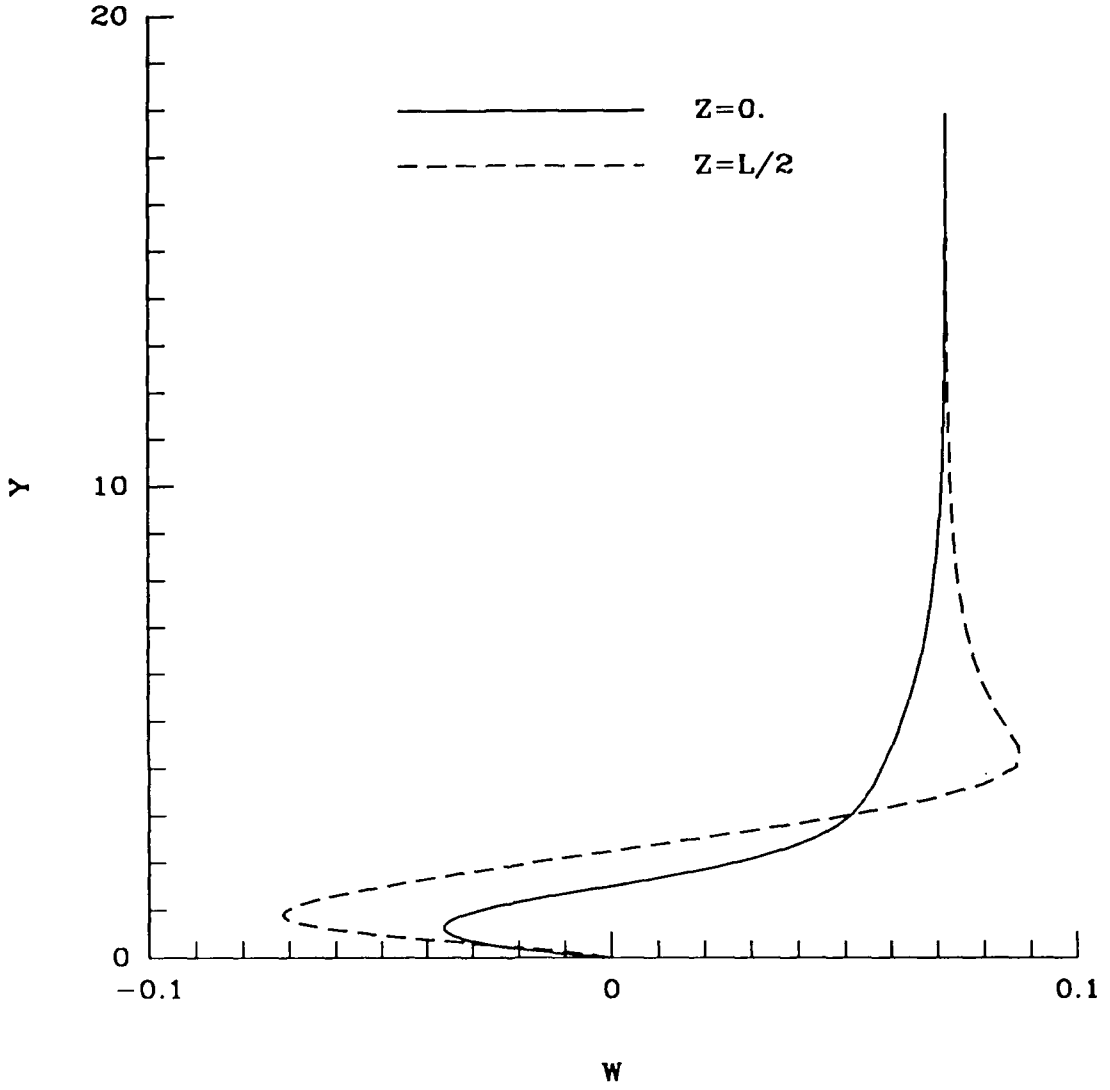

(b) velocity component in the direction at 90° to the crossflow vortex axis

Figure 24. Concluded.

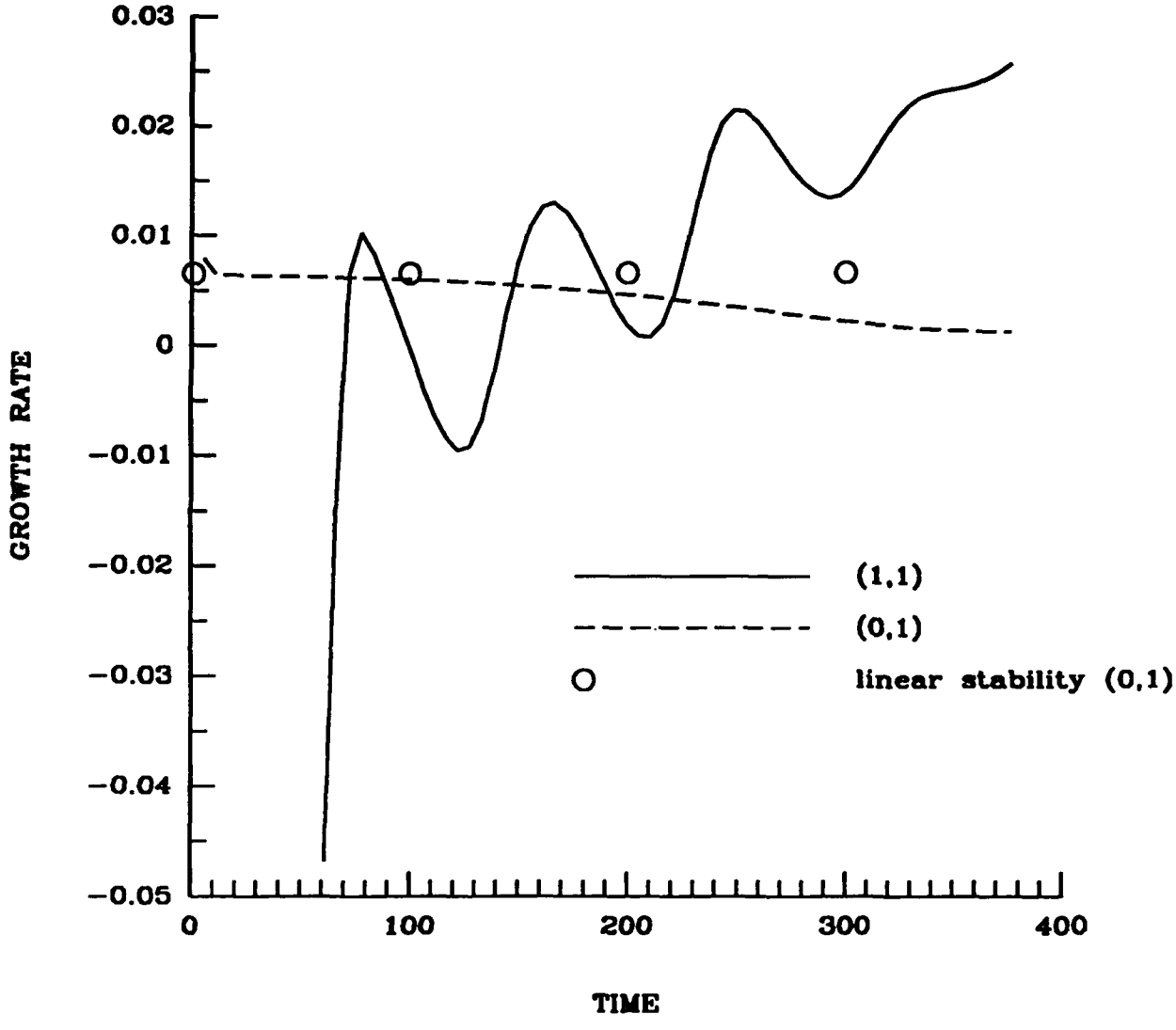

Figure 25. Growth rates of various modes in the presence of a finite amplitude crossflow vortex in FSC boundary layer.